The Astrophysical Journal, 570:671–687, 2002 May 10

A *CHANDRA* STUDY OF SAGITTARIUS A EAST: A SUPERNOVA REMNANT REGULATING THE ACTIVITY OF OUR GALACTIC CENTER?

Y. Maeda,[1,2] F. K. Baganoff,[3] E. D. Feigelson,[1] M. Morris,[4] M. W. Bautz,[3] W. N. Brandt,[1] D. N. Burrows,[1] J. P. Doty,[3] G. P. Garmire,[1] S. H. Pravdo,[5] G. R. Ricker,[3] and L. K. Townsley[1]

Received 2000 November 9; accepted 2002 January 22

ABSTRACT

We report on the X-ray emission from the shell-like, nonthermal radio source Sgr A East (SNR 000.0+00.0), located in the inner few parsecs of the Galaxy based on observations made with the ACIS detector on board the *Chandra X-Ray Observatory*. This is the first time Sgr A East has been clearly resolved from other complex structures in the region. The X-ray–emitting region is concentrated within the central $\simeq$2 pc of the larger radio shell. The spectrum shows strong Kα lines from highly ionized ions of S, Ar, Ca, and Fe. A simple isothermal plasma model gives electron temperature $\sim$2 keV, absorption column $\sim 1 \times 10^{23}$ H cm^{-2}, luminosity $\sim 8 \times 10^{34}$ ergs s^{-1} in the 2–10 keV band, and gas mass $\sim 2\eta^{1/2}\ M_{\odot}$ with a filling factor η. The plasma appears to be rich in heavy elements, overabundant by roughly a factor of 4 with respect to solar abundances, and shows a spatial gradient of elemental abundance; the spatial distribution of iron is more compact than that of the lighter elements. The gas mass and elemental abundance of the X-ray emission support the long-standing hypothesis that Sgr A East is a supernova remnant (SNR), perhaps produced by the Type II supernova explosion of a massive star with a main-sequence mass of 13–20 $M_{\odot}$. The combination of the radio and X-ray morphologies classifies Sgr A East as a new metal-rich "mixed morphology" (MM) SNR. The size of the Sgr A East radio shell is the smallest of the known MM SNRs, which strongly suggests that the ejecta have expanded into a very dense interstellar medium. The ejecta-dominated chemical compositions of the plasma indicate that the ambient materials should be highly homogeneous. We thus evaluate a simplified dynamical evolution model where an SNR was formed about 10,000 yr ago and expanded into an ambient medium with a homogeneous density of 10^3 cm^{-3}. The model roughly reproduces most of the observed properties in the X-ray and radio wavelengths. A comparison with the radio observations requires the dense ambient medium to be ionized, but a luminous X-ray irradiator with an expected X-ray luminosity of $\sim 10^{40}$ ergs s^{-1} is not currently present. The presence of the ionized gas may be explained if the massive black hole (MBH) associated with the compact, nonthermal radio source Sgr A* was bright in X-rays about 300 yr ago but is presently dim. It is possible that the dust/molecular ridge compressed by the forward shock of Sgr A East hit Sgr A* in the past, and the passage of the ridge may have supplied material to accrete onto the black hole in the past and may have removed material from the black hole vicinity, leading to its present quiescent state. This may be a specific example of the intimate relationship between an SNR and MBH accretion activity in galactic nuclei.

Subject headings: Galaxy: center — ISM: individual (Sagittarius A East) — supernova remnants — X-rays: ISM

1. INTRODUCTION

The center of our Galaxy embodies a rich variety of phenomena that create diverse complex structures that are visible to us over a broad range of wavelengths. The radio emission from the central few parsecs of the Galaxy has several components, including a compact nonthermal source (Sgr A*) thought to be associated with the central massive black hole (MBH), a spiral-shaped group of thermal gas streams (Sgr A West) that are possibly infalling to Sgr A*, and a $3\farcm5 \times 2\farcm5$ shell-like nonthermal structure (Sgr A East; Ekers, Goss, & Schwarz 1975; see also Fig. 1). Sgr A East surrounds Sgr A*/West in projection, but its center is offset by about 50″ (2 pc). A number of arguments suggest that Sgr A* West is physically located very near or possibly embedded within Sgr A East. For the latter case, interaction between Sgr A East and Sgr A*/West would be inevitable, so Sgr A East may be a key for understanding the activity in the nucleus of our Galaxy (for a recent review, see Yusef-Zadeh, Melia, & Wardle 2000).

Radio studies indicate that Sgr A East may be interpreted simply as a supernova remnant (SNR 000.0+00.0; Jones 1974; Ekers et al. 1983; Green 1984). However, its location extremely close to the Galactic nucleus and its inferred energetics have inspired alternative interpretations, for example, multiple SNRs or the remnant of an extremely energetic explosion owing to tidal disruption of a star by the central massive black hole (Yusef-Zadeh & Morris 1987; Mezger et al. 1989; Khokhlov & Melia 1996). Thus, the origin of Sgr A East is still an open issue.

The nonthermal radio emission from the Sgr A East shell, owing to synchrotron radiation from relativistic electrons, has an unusually high surface brightness for a Galactic SNR and is an outlier in the Σ-D relation (Green 1984; Case & Bhattacharya 1998). Yusef-Zadeh et al. (1996) found a possible Zeeman-split OH maser line arising in the com-

[1] Department of Astronomy and Astrophysics, 525 Davey Laboratory, Pennsylvania State University, University Park, PA 16802-6305.

[2] Present Address: Institute of Space and Astronautical Science, 3-1-1 Yoshinodai, Sagamihara, Kanagawa 229-8510, Japan; ymaeda@astro.isas.ac.jp.

[3] Massachusetts Institute of Technology, Center for Space Research, 77 Massachusetts Avenue, Cambridge, MA 02139-4307.

[4] Division of Astronomy, Box 951562, UCLA, Los Angeles, CA 90095-1562.

[5] Jet Propulsion Laboratory, MS 306-438, 4800 Oak Grove Drive, Pasadena, CA 91109.

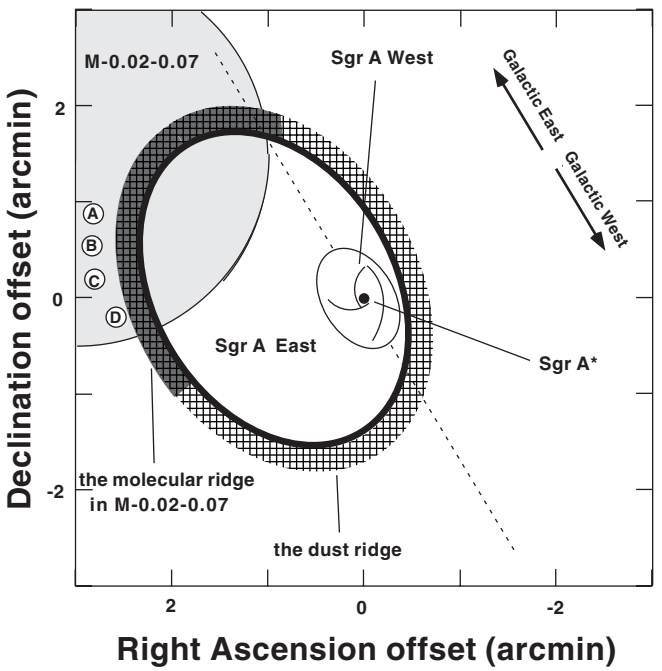

FIG. 1.—Schematic diagram showing the sky locations and rough sizes and shapes of Galactic center sources (e.g., Yusef-Zadeh et al. 2000). The coordinate offsets are with respect to the compact nonthermal radio source Sgr A*, which coincides with the MBH. Sgr A* is located at the center of the thermal radio source Sgr A West, which consists of a spiral-shaped group of thermal gas filaments. Sgr A West is surrounded by the molecular ring (also known as the circumnuclear disk), the radius of which is about 30″. The nonthermal shell-like radio source Sgr A East discussed here is surrounding Sgr A West, but its center is offset by about 50″. The nonthermal shell is surrounded by the dust and the molecular ridge. The molecular cloud $M-0.02-0.07$ (the $+50$ km s^{-1} cloud) is located to the Galactic east of Sgr A East. The molecular ridge is also classified as a part of $M-0.02-0.07$ because both of the peak velocities in molecular lines appear around $+50$ km s^{-1}. At the eastern edge of the Sgr A East shell, the chain of H II regions (A–D) is seen. One arcminute corresponds to about 2.3 pc at the distance of 8 kpc.

pressed dust/molecular ridge outside this nonthermal radio shell, and they inferred a magnetic field strength of 2–4 mG. This strong magnetic field may cause unusually rapid synchrotron aging. Regardless of what actually caused the initial explosion, the coexistence of the relativistic particles and the strong magnetic field indicates Sgr A East is a unique particle accelerator in the Galaxy (e.g., Yusef-Zadeh et al. 2000). The age and the shock velocity of Sgr A East are crucial parameters for determining the energy distribution of the accelerated particles (Sturner et al. 1997 and references therein), which leads in turn to a better understanding of how Sgr A East may contribute cosmic rays and γ-ray emission to the Galactic center maelstrom.

Sgr A East appears to be interacting with the $+50$ km s^{-1} molecular cloud ($M-0.02-0.07$), and it has been suggested by others that it could have stimulated star formation as evidenced by a chain of compact H II regions located just to the east in projection (Goss et al. 1985; Ho et al. 1985; Yusef-Zadeh & Mehringer 1995; Novak et al. 2000; see also Fig. 1). Cotera et al. (1999) found an infrared star positionally coincident with one of the H II regions. They estimated that the star might be in the Wolf-Rayet phase (WN7), so if the H II region was created by an interaction with the Sgr A East shell, then Sgr A East would have to be over $\sim 10^5$–10^6 yr old. However, Uchida et al. (1998) showed that the shear associated with nonsolid Galactic rotation causes distortion of an expanding bubble in the Galactic longitudinal direction. The elongated radio structure of Sgr A East is naturally reproduced on relatively short timescales of $\sim 10^4$ yr, and it would be sheared out of existence in $\sim 10^5$ yr.

In the soft X-ray band, enhanced emission from the vicinity of Sgr A East is evident in a *ROSAT* image, but it was not studied (Predehl & Trümper 1994). In the hard 2–10 keV band, an *ASCA* image showed an oval-shaped region of $2' \times 3'$ filling the Sgr A radio shell (Koyama et al. 1996) with a surface brightness 5 times that of the surrounding diffuse emission. The absorption column density and the luminosity from the oval-shaped region were found to be approximately 7×10^{22} cm^{-2} and 10^{36} ergs s^{-1}. With *BeppoSAX* data, Sidoli et al. (1999) reported that the spectrum of the emission integrated over the entire Sgr A region can be modeled with a multitemperature thermal plasma or a combination of nonthermal and thermal emission with prominent emission lines at 2.4 keV from S Kα and at 6.7 keV from highly ionized Fe Kα (Sidoli et al. 1999; Sidoli & Mereghetti 1999). However, the $\sim 1'$ spatial resolution of *ASCA* and *BeppoSAX* could not establish the detailed X-ray properties of the Sgr A region.

The *Chandra X-ray Observatory* (*Chandra*) with the Advanced CCD Imaging Spectrometer (ACIS) detector combines the wide-band sensitivity and moderate spectral resolution of the *ASCA* and *BeppoSAX* satellites with the much higher spatial resolution (0.″5–1″) of *Chandra*'s high-resolution mirror assembly (HRMA). ACIS clearly resolved Sgr A East from its complex environs. Baganoff et al. (2001, hereafter Paper I) provides an overview of our findings for the entire $17'$ ($\approx$40 pc) ACIS-I field of view and discusses the X-ray emission from the immediate vicinity of the MBH at Sgr A*. This paper focuses on a detailed analysis of Sgr A East. Throughout this paper we adopt a distance of 8.0 kpc to the Galactic center (Reid 1993).

2. OBSERVATIONS AND ANALYSIS PROCEDURES

2.1. *Data Acquisition and Reduction*

The observation of Sgr A was carried out early in the *Chandra* mission on 1999 September 21 (ObsID 242) over a period of 51.1 ks using the ACIS-I array of four abutted, frontside-illuminated CCDs. The satellite and instrument are described by Weisskopf, O'Dell, & van Speybroeck (1996) and G. Garmire, J. Nousek, & M. Bautz (2002, in preparation), respectively.[6] The telemetry limit of the satellite was exceeded during $\sim$21% of the observation owing to high background caused by the impact of energetic solar particles on the CCDs. Exposure frames were dropped during telemetry saturation, causing irretrievable loss of information. The effective exposure time was 40.3 ks. The Sgr A complex was imaged near the center of the ACIS-I array of four 1024×1024 pixel CCDs, each with $0.''5 \times 0.''5$ pixels and a field of view of $8.'4 \times 8.'4$. Data acquisition with ACIS was made in timed-exposure (TE) very faint (VF) mode with chip readout every 3.24 s. The focal plane temperature was about -110°C.

Individual events were preprocessed on board using a lower event threshold of 38 ADU and a "split" threshold of 13 ADU. Events with ACIS flight grades of 24, 66, 107, 214, or 255, and those occurring in known bad pixels and

[6] Details about ACIS can be found at http://www.astro.psu.edu/xray/axaf.

columns, were removed on board to reduce telemetry. The celestial coordinates of events were determined during ground-based processing based on guide-star aspect solutions, improved by alignment to astrometric standard stars as described in Paper I.

Early in the mission, the ACIS frontside-illuminated CCDs suffered a significant increase in parallel charge transfer inefficiency (CTI) because of radiation damage acquired during satellite perigee passages through the terrestrial radiation belts (Prigozhin et al. 2000). The CTI causes a progressive row-dependent decrease in the detection efficiency and energy gain accompanied by a degradation of the energy resolution. Sgr A East was imaged near the top of amplifier 3 on chip I3, a location known to be heavily affected by CTI. To mitigate the energy bias and recover from grade migration caused by CTI, we applied the software corrector described by Townsley et al. (2000).

The conversion from event ADU to photon energy used in our spectral analysis uses a response matrix based on a nearly contemporaneous observation of reference radioactive and fluorescent emission lines from an on-board calibration source (ObsID 1310), which were processed with the same CTI corrector. From analysis of the instrumental Ni-Kα (7.5 keV) and Au-Lα (9.7 keV) lines arising from particle bombardment of satellite metals, we found the energies are probably underestimated by $\sim$100 eV at $E \geq 7$ keV. Thus, we removed a $\sim$2% bias in the energy gain at the chip location of Sgr A.

Further analysis of the calibration lines indicates that the detection efficiency in the low-energy band ($\sim$2 keV) is almost flat across each CCD, while it is significantly decreased in the high-energy band toward the top rows of each chip. The effective area of the telescope mirrors and the detection efficiency of ACIS were calculated with the MKARF program in the *Chandra* Interactive Analysis of Observations Software package (CIAO version 1.0), which, at the present time, does not account for the positional dependence of the detection efficiency owing to the CTI effects. We estimate that this could cause the inferred temperatures to be systematically lower than the true temperatures by $\sim$10% at $kT_e = 2$ keV. We do not remove this bias in the analysis below.

To reject background events, we applied a grade filter to keep only *ASCA* grades 0, 2, 3, 4, and 6. We removed events from flaring pixels using the "flagflare" routine written by T. Miyaji. Artificial stripes caused probably by hot pixels in the frame-store region and by particles which hit on the CCD node boundaries were also removed.[7]

2.2. *Image Flat-Fielding*

Figure 2*a* shows a broadband raw count image of the Sgr A region between 1.5 and 7 keV. To visualize better the complex combination of extended and compact structures

[7] Detailed procedures for cleaning low-quality events are given in http://www.astro.psu.edu/xray/axaf/recipes/clean.html.

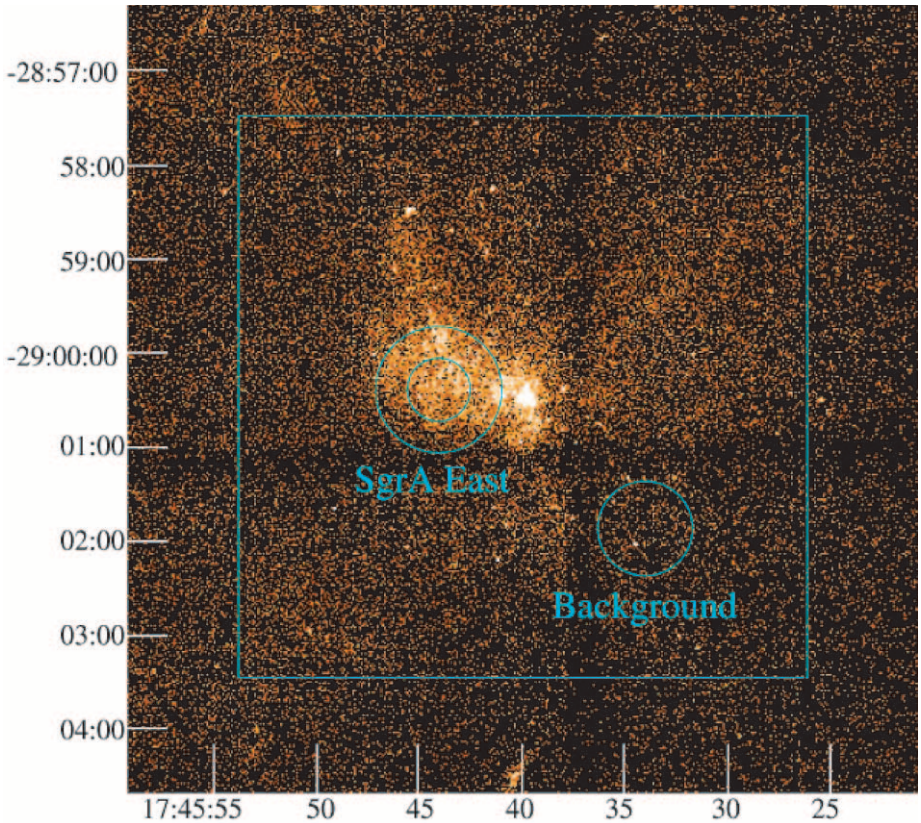

FIG. 2*a*

FIG. 2.—(*a*) Raw image in the 1.5–7.0 keV band binned by a factor of 2 pixels. The grids are the FK5 coordinates R.A., decl. (J2000). Neither exposure nor vignetting correction is applied. Circles correspond to the regions from which spectra were taken. The outer circle of the Sgr A East region is used for the analysis of the overall spectrum, while the inner circle is used to test radial dependence of the spectrum. The large square corresponds to the scale of the schematic diagram given in Fig. 1. (*b–e*) Smoothed images in the (*b*) 1.5–7.0, (*c*) 1.5–3.0, (*d*) 3.0–6.0, and (*e*) 6.0–7.0 keV bands. Both exposure and vignetting corrections were applied. The large and small white dashed ellipses approximately represent the Sgr A East nonthermal shell and an outer boundary of the Sgr A West region, respectively. In all the panels, the field center is at Sgr A*, and the panel size is $8'.4 \times 8'.4$.

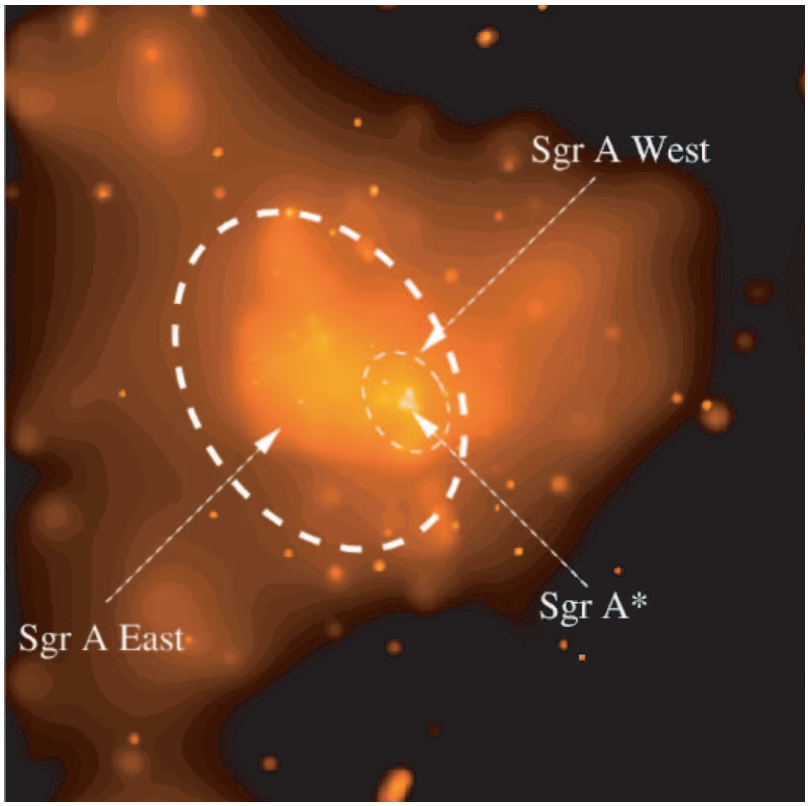

FIG. 2*b*

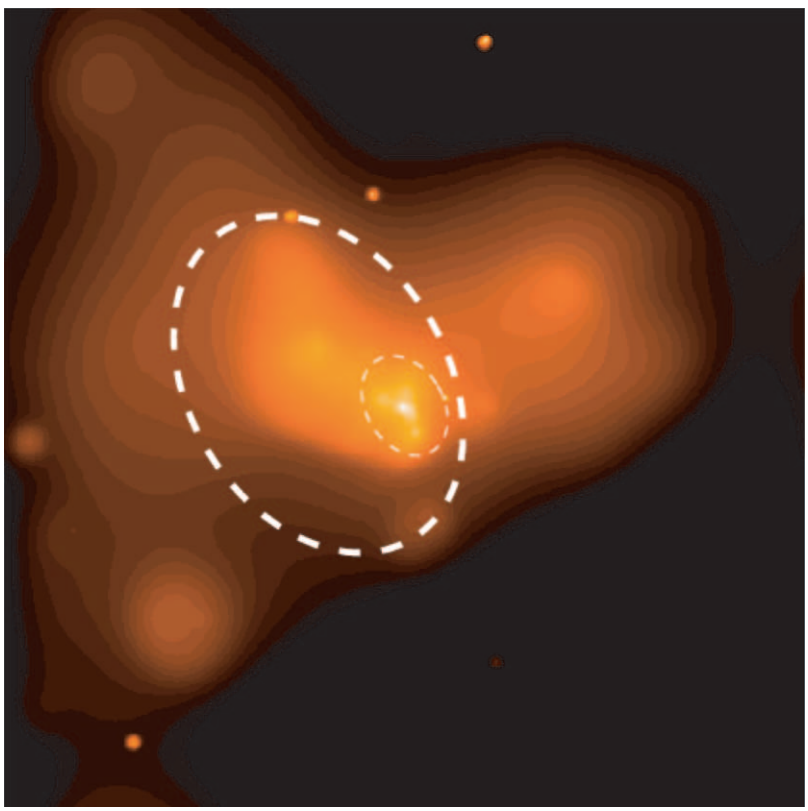

FIG. 2*c*

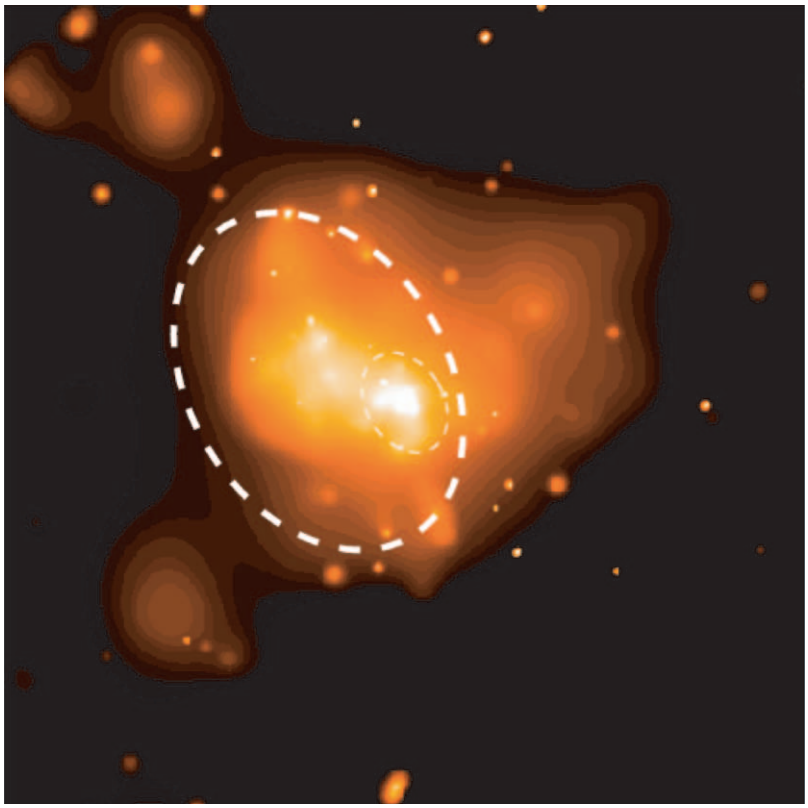

FIG. 2*d*

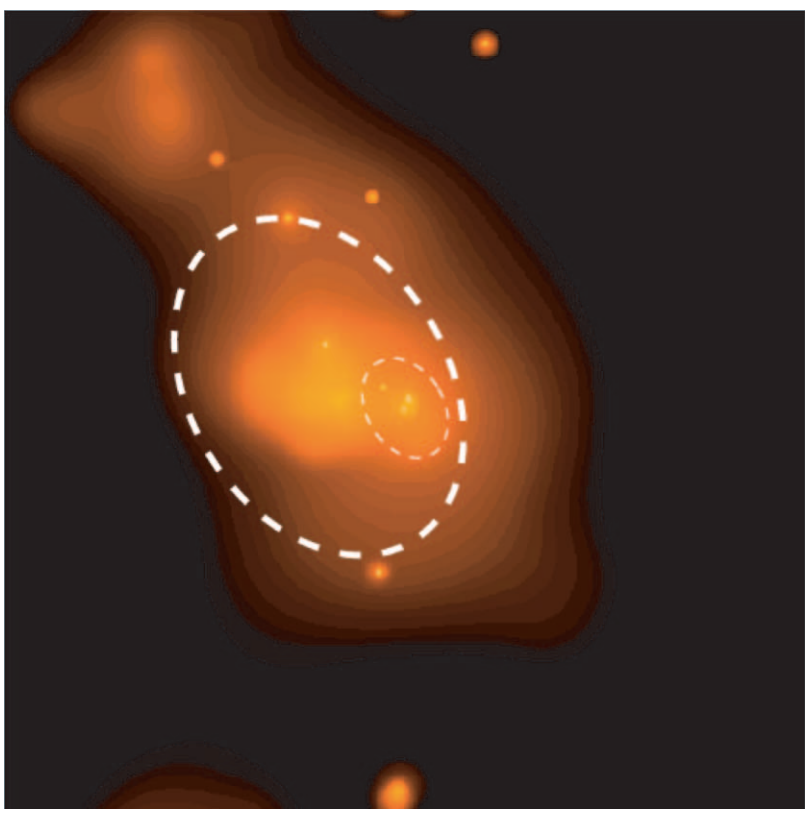

FIG. 2*e*

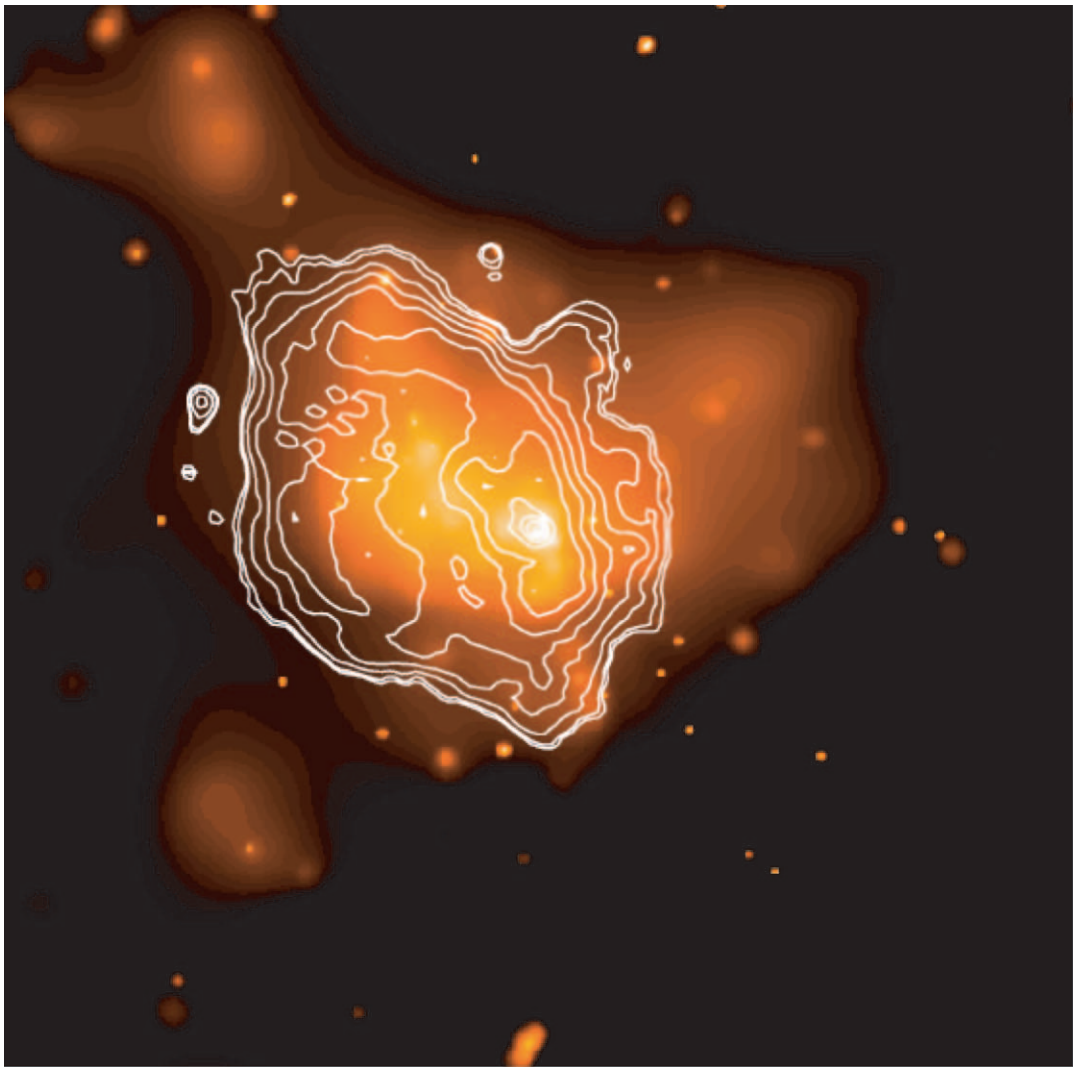

FIG. 3.—Smoothed X-ray image (1.5–7.0 keV) with 20 cm radio contours (*white*: F. Yusef-Zadeh 2001, private communication)

in the region, we apply an adaptive kernel smoothing algorithm developed by Ebeling, White, & Rangarajan (2002) to the raw count image. This algorithm uses the local density of events to determine the width of the Gaussian smoothing kernel at each location across the image. However, smoothing the raw count image convolves the diminished event density owing to gaps between the CCDs (which are already broadened by satellite dithering) with real astrophysical structures.

To remove this instrumental effect, we create an exposure map and adaptively smooth it using a map of the kernel widths used by the algorithm to smooth the count map. We then divide the smoothed image by the smoothed exposure map to remove instrumental effects owing to mirror vignetting and the interchip gaps; this yields a flat-fielded smoothed X-ray flux map.

As the effective area varies from region to region and from energy to energy, this method is valid only for a narrowband image. In order to make a broadband image spanning 1.5–7 keV, we adaptively smooth the 1.5–7 keV image to get a map of kernel widths, and use this kernel map to smooth images and exposure maps in three narrow bands: 1.5–3.0, 3.0–6.0, and 6.0–7.0 keV. We then divide the smoothed image in each band by the appropriate smoothed exposure map to create three flat-fielded narrowband flux maps (see Figs. 2*c*–2*e*). Finally, we sum the narrowband flux maps to produce the broadband map (see Fig. 2*b* and Fig. 3). A typical Gaussian width for the smoothing is about 5″ at the center of Sgr A East. Ratios among the three bands provide the hardness ratio maps shown in Figure 4.

2.3. *Point-Source Removal*

Several dozen pointlike sources can be seen in Figure 2. To study the diffuse components in and around Sgr A East, we removed these pointlike sources. Source detection is based on a Mexican hat wavelet decomposition of the unsmoothed image using the WAVDETECT program in the CIAO software package (Freeman et al. 2002). The source detection threshold was set at 10^{-6}, corresponding to $\sim$1 spurious source per chip. The wavelet scales used were 1, $\sqrt{2}$, 2, $2\sqrt{2}$, 4, $4\sqrt{2}$, 8, $8\sqrt{2}$, and 16 pixels. For the analysis of extended features, we excluded all events lying within an 8 σ radius of each compact source, where σ is the standard deviation of the telescope point-spread function at 1.5 keV at each location. This should remove greater than 90% of the point source photons.

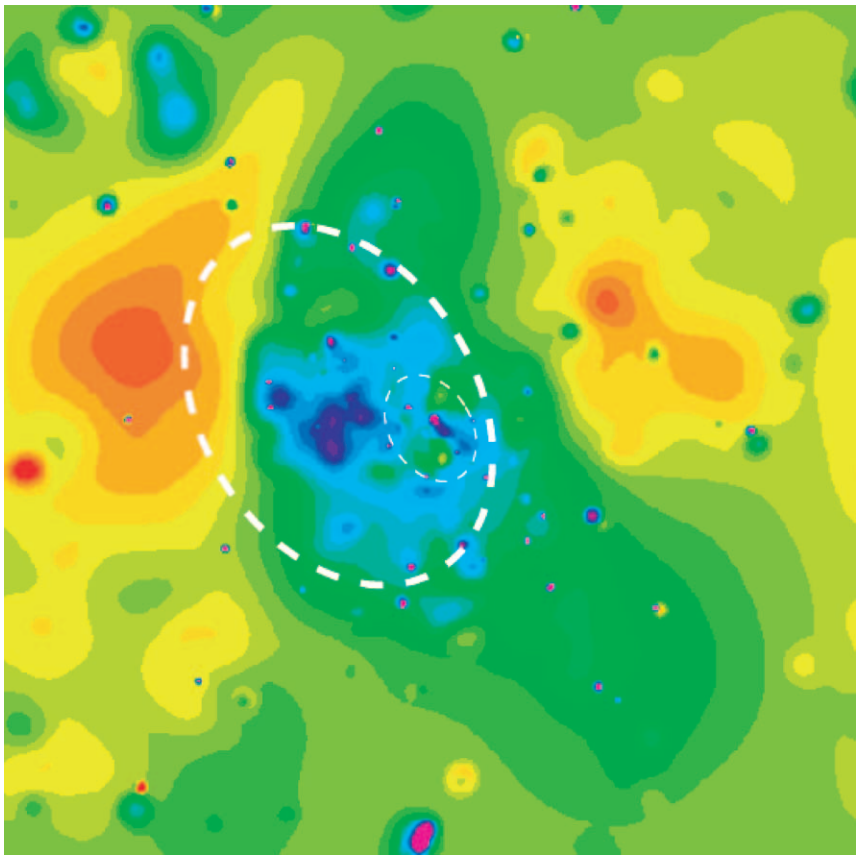

FIG. 4*a*

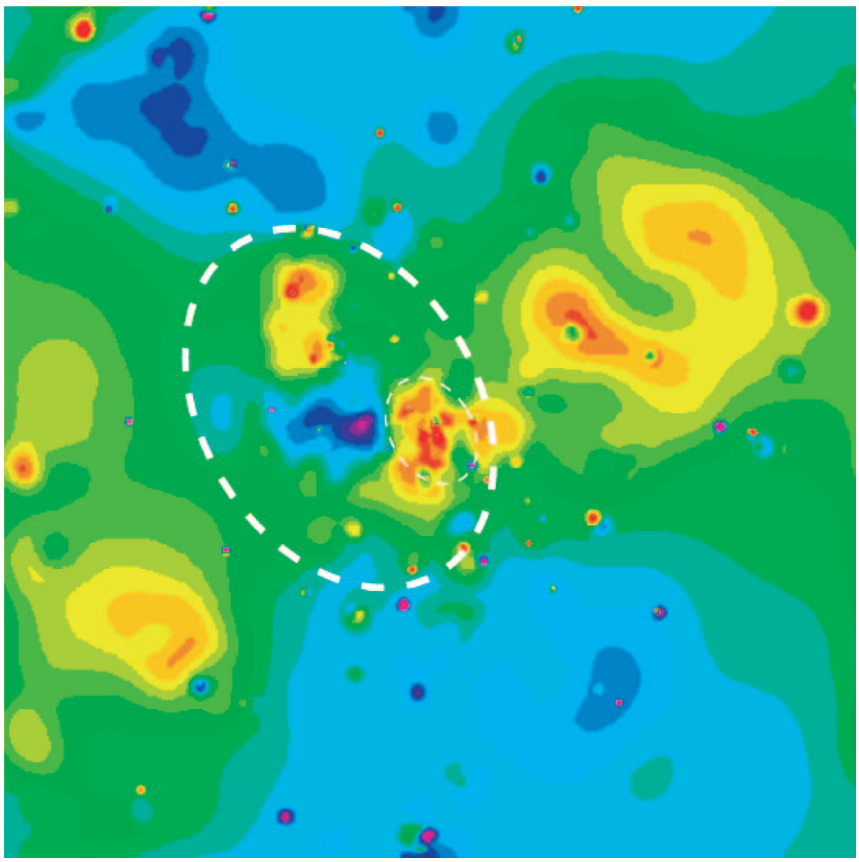

FIG. 4*b*

FIG. 4.—Hardness ratio map of the smoothed images. The blue color indicates hardness, while the red implies softness. (*a*) (3.0–6.0 keV)/(1.5–3.0 keV); (*b*) (6.0–7.0 keV)/(3.0–6.0 keV).

3. X-RAY PROPERTIES

3.1. *Morphology*

Raw and smoothed broadband (1.5–7 keV) X-ray images of the Sgr A radio complex are shown in Figures 2*a* and 2*b*. Dozens of point sources and complex extended structures are clearly seen, as reported in Paper I. In Figure 3, we show the smoothed broadband X-ray image overlaid with radio contours from a 20 cm Very Large Array image of Sgr A provided to us by F. Yusef-Zadeh. The outer oval-shaped contours are due to synchrotron emission from the shell-like nonthermal radio source Sgr A East, which may be a supernova remnant (SNR 000.0+00.0; Ekers et al. 1983; Green 1984). The thermal radio source Sgr A West, an H II region located in the central parsecs of the Galaxy, appears on the western side of the Sgr A complex. At 90 cm, the nonthermal emission from Sgr A East is seen to be absorbed by the ionized gas in Sgr A West, which must therefore be located along the line of sight between us and Sgr A East (Yusef-Zadeh & Morris 1987; Pedlar et al. 1989; Anantharamaiah, Pedlar, & Goss 1999).

Several bright compact X-ray sources can be seen in the vicinity of Sgr A West. One of these sources is coincident to within $0\farcs35$ with the radio position of the compact nonthermal radio source Sgr A*. Analysis of the X-ray emission from this source and its vicinity is reported in Paper I. In addition to the compact sources, the Sgr A West region shows bright diffuse X-ray emission superposed on a broader region of extended emission, which peaks $\sim1'$ east of Sgr A* and which appears to fill the central ~2 pc of the Sgr A East radio shell (Fig. 3). This broader feature is especially conspicuous in the 6–7 keV band (Fig. 2*e*), where the flux is dominated by iron-K line emission (§ 3.2). Notably, no significant X-ray continuum or line emission is seen from the location of the radio shell. On the basis of its spectral and spatial properties, we associate the source of this diffuse X-ray emission with a hot optically thin thermal plasma located within the Sgr A East radio shell.

A curious linear feature $\sim0\farcm5$ long, which we refer to as the "plume" in Paper I, can be seen extending (in projection) from the center of Sgr A East to the northwest. This feature is most obvious in the 3–6 keV band (Fig. 2*d*). The total count rate from the plume is only 5%–10% of that from Sgr A East. Although it is possible that the plume is physically associated with Sgr A East, our results on the spectral properties of Sgr A East given in this paper are unchanged by the inclusion, or not, of the flux in the plume. Looking in the 1.5–3 keV band (Fig. 2*c*), we clearly see faint X-ray emission extending perpendicular to the Galactic plane in both directions through the position of Sgr A*. This emission is not apparent in the 6–7 keV map and therefore appears to be unrelated to Sgr A East. The two-sided nature of this emission suggests it might originate in some kind of bipolar outflow. Results of a detailed analysis of the X-ray emission from these structures will be published elsewhere.

The total surface brightness in the direction of Sgr A East is $\sim4.3 \times 10^{-5}$ counts s^{-1} arcsec^{-2}. This was measured by extracting counts from a circular region of radius $40''$ centered at (R.A., decl.)$_{J2000}$ = ($17^h45^m44\fs1$, $-29°00'23''$), as shown in Figure 2*a*. A total of 8700 counts were extracted, corresponding to a count rate of 0.22 counts s^{-1}. The entire Sgr A region is surrounded by diffuse emission that varies considerably in intensity and spectrum. It is thus difficult to determine exactly what background to subtract. We chose to estimate the background using the counts within a $30''$ radius circular region centered at (R.A., decl.)$_{J2000}$ = ($17^h45^m34\fs0$, $-29°01'52''$). A total of 708 counts were extracted in the 1.5–9 keV band from the background region, yielding a surface brightness of $\sim6.1 \times 10^{-6}$ counts s^{-1} arcsec^{-2}. If this diffuse emission is assumed to be roughly constant at Sgr A East, then the estimated background rate within the source region is 3.1×10^{-2} counts s^{-1}. The net surface brightness and count rate from Sgr A East are then $\sim3.6 \times 10^{-5}$ counts s^{-1} arcsec^{-2} and 0.18 counts s^{-1}.

From the smoothed images in different energy bands, we found that the structure of the Sgr A East emission is spectrally dependent. The half-power radius of the emission is $\sim20''$ in the 6–7 keV band compared to $\sim30''$ in the lower energy bands. The concentration of hard emission toward the center can be seen in the hardness-ratio maps of Figure 4, which show structure on scales of $10''$–$20''$ toward the center of Sgr A East.

3.2. *Spectra*

In order to quantitatively evaluate the spectrum of Sgr A East, we extracted source and background spectra from the regions described in § 3.1. As noted above, the diffuse emission surrounding the Sgr A region varies considerably in intensity and spectrum. Thus, there is some uncertainty inherent in the background subtraction. Using the spectrum extracted from a second background region centered at (R.A., decl.)$_{J2000}$ = ($17^h45^m50\fs6$, $-29°01'46''$), we found that the net emission derived for the low-energy band around 2 keV depends somewhat on the choice of background, while the emission in the harder bands is reasonably secure. Our analysis indicates that none of the scientific conclusions discussed in this paper are dependent on the background subtraction. The background-subtracted count rate for the $40''$ radius emission is 0.03, 0.12, and 0.03 counts s^{-1} in the 1.5–3.0, 3.0–6.0, and 6.0–9.0 keV bands, respectively.

The spectrum of Sgr A East, shown in Figure 5, exhibits continuum plus emission lines that give critical information on the physical state of the plasma. We first fit the spectrum with a thermal bremsstrahlung model having four Gaussian emission lines of unspecified energy, all absorbed by an interstellar medium (ISM) having cosmic abundances. The best-fit parameters are shown in Table 1. The emission lines can be attributed to the Kα transitions of the helium-like ions of sulfur, argon, calcium, and iron. The line width for each line is consistent with being unresolved. The existence of the highly ionized ions confirms the presence of an optically thin thermal plasma. The equivalent widths of the lines are relatively small for the first three elements (EW $\simeq$ 0.1–0.2 keV) but very large for iron (EW $\simeq$ 3.1 keV). The continuum temperature is around 3 keV, and the line-of-sight column density is around 1×10^{23} cm^{-2}, equivalent to a visual absorption of $A_V \simeq 60$ mag (we assume $N_H = 1.79 \times 10^{21} A_V$; Predehl & Schmitt 1995).

The large equivalent width of the iron line suggests that the Sgr A East plasma is enriched in heavy elements. Since the high-ionization state of the iron K line can be reproduced by a plasma in collisional ionization equilibrium (Masai 1994), we fit the spectrum to models of an isothermal plasma having variable elemental abundances (MEKA; Mewe, Gronenschild, & van den Oord 1985), modified by interstellar absorption. The model with solar elemental abundances (Anders & Grevesse 1989) was rejected with

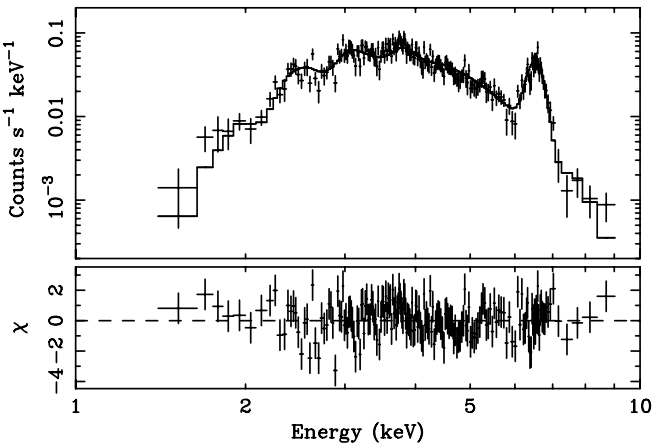

FIG. 5.—ACIS-I spectrum of Sgr A East. Error bars are 1 σ. The solid line corresponds to the best-fit value with the MEKA model summarized in Table 2. Fit residuals are shown in the bottom panel.

$\chi^2 = 309$ (185 degrees of freedom) because it does not reproduce the large equivalent width of the iron line. The best fit ($\chi^2 = 217$ with 184 dof) was obtained using heavy element abundances that are $\simeq$4 times solar. These results are given in Table 2 and are shown as a solid line in Figure 5.

In order to examine relative abundances among heavy elements, we allowed only the iron abundance $Z_{\rm Fe}$ to be a free parameter, fixing the hydrogen abundance at zero and holding other elements, $Z_{\rm others}$ at their solar ratios. The best fit (χ^2/dof = 218/184) does not indicate that iron is more overabundant than other metals: $z_{\rm Fe} \equiv Z_{\rm Fe}/Z_{\rm others} = 1.1$ (1.0–1.4).

Assuming energy equipartition between electrons and ions, the best-fit model gives the following physical properties for the plasma, assuming a spherical volume with radius 1.6 pc and an unknown filling factor η: electron density $n_e \simeq 6\eta^{-1/2}$ cm^{-3}, gas mass $M_g \simeq 2\eta^{1/2}\, M_\odot$, X-ray luminosity $L_{\rm X} \simeq 8 \times 10^{34}$ ergs s^{-1} in the 2–10 keV band,[8] and total thermal energy $2 \times 10^{49}\eta^{1/2}$ ergs.

For a quantitative analysis of the radial dependence of the spectra, we divided the Sgr A East region into two concentric annuli, each with a 20″ width (Fig. 2*a*), and obtained X-ray spectra from each annulus (Fig. 6). We fitted the spectra with the absorbed thermal bremsstrahlung plus Gaussians model, fixing the line energies to be those given in Table 1. The best-fit parameters are plotted in Figure 7. The most striking spatial variation is that the equivalent width of iron in the inner region is elevated by a factor of 1.5 compared to the surrounding region, while the equivalent widths of sulphur, argon, and calcium are consistent with being uniform. The electron temperature also appears constant between the two regions. The relative abundance $z_{\rm Fe}$ of iron compared to other metals in the MEKA model assuming the temperature and the absorption are the same in the two regions shows 2.2(1.7–2.8) and 0.8(0.7–1.0) for the inner and outer regions, respectively (χ^2/dof = 331/295). Even if we allow temperature and absorption to vary, the abundance gradient is present with 3 σ confidence. We

[8] Here and elsewhere, $L_{\rm X}$ is the absorption-corrected luminosity in the 2–10 keV band unless otherwise noted.

TABLE 1
BEST-FIT PARAMETERS TO THE SGR A EAST SPECTRUM FITTED WITH A THERMAL BREMSSTRAHLUNG WITH FOUR GAUSSIANS

Continuum			
Parameter			Value
$N_{\rm H}$ ($\times 10^{22}$ cm^{-2})			9.4(8.7–10.2)
kT_e (keV)			3.0(2.6–3.5)
Emission Lines			
Line Energy (keV)	Line ID (keV)[a]	I (10^{-5} photons cm^{-2} s^{-1})[b]	EW (eV)[c]
2.49 (2.45–2.53)	S XV (2.45)	0.9 (0.5–1.4)	140
3.16 (3.10–3.23)	Ar XVII (3.14)	1.1 (0.7–1.6)	92
3.85 (3.81–3.88)	Ca XIX (3.90)	2.2 (1.7–2.6)	173
6.69 (6.67–6.71)	Fe XXV (6.67)	12.2 (11.2–13.2)	3100
2–10 keV Band			
Parameter			Value
$F_{\rm X}$ (ergs cm^{-2} s^{-1})			5×10^{-12}
$L_{\rm X}$ (ergs s^{-1})			8×10^{34}
χ^2(dof)			190(177)

NOTE.—No systematic error was included in the values given in the table. See the text for the error. X-ray flux ($F_{\rm X}$) is not corrected for absorption, while luminosity ($L_{\rm X}$) is corrected. All the errors given in parentheses are for 90% confidence level. A narrow line is assumed.

[a] Line identification. Theoretical energy of a Kα transition line (Mewe et al. 1985) is given in parentheses.

[b] Line flux.

[c] Equivalent width.

TABLE 2
BEST-FIT PARAMETERS TO THE SGR A EAST SPECTRUM FITTED WITH THE MEKA MODEL

Parameter	Best-Fit Value
$N_{\rm H}$ ($\times 10^{22}$ cm^{-2})	11.4 (10.5–12.3)
kT_e (keV)	2.1 (1.9–2.4)
Z	3.9 (2.9–5.9)
Normalization	1.1 (0.9–1.3)
χ^2 (dof)	217 (184)

NOTE.—Normalization: $10^{-12} \int n_e n_{\rm H} dV / (4\pi D^2)$, where n_e is the electron number density (cm^{-3}), $n_{\rm H}$ is the proton number density (cm^{-3}), and D is the distance to the source (cm); $n_e = 1.8 \times n_{\rm H}$ for the best fit.

thus conclude that iron is concentrated in the interior region by a factor of $\sim$2, while the lighter elements are spatially roughly homogeneous.

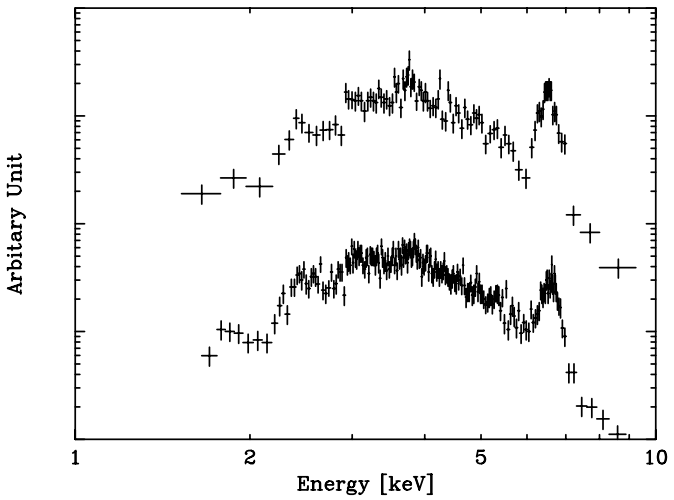

FIG. 6.—Spectra taken from two regions of Sgr A East. The upper spectrum is for the circular region with a radius of 20″, while the lower is for the outer annular region with inner and outer radii of 20″ and 40″. The unit in the vertical axis is arbitrary.

4. DISCUSSION

4.1. *Origin of Sgr A East*

The X-ray spectrum enriched by heavy elements suggests that the X-ray plasma is dominated by supernova ejecta. The small gas mass of $2\eta^{1/2}\ M_\odot$ and thermal energy $\sim 10^{49}$ ergs are consistent with the ejecta by a single supernova explosion. These results straightforwardly supports the long-standing hypothesis that Sgr A East is a single SNR (Ekers et al. 1983).

Rho & Petre (1998) defined a new class of composite SNRs showing centrally concentrated thermal X-rays lying

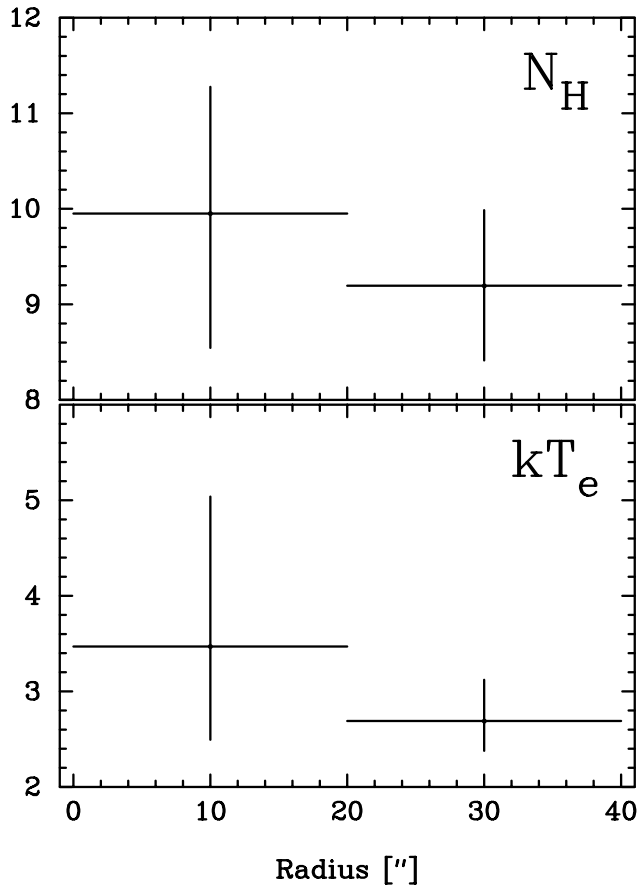

FIG. 7*a*

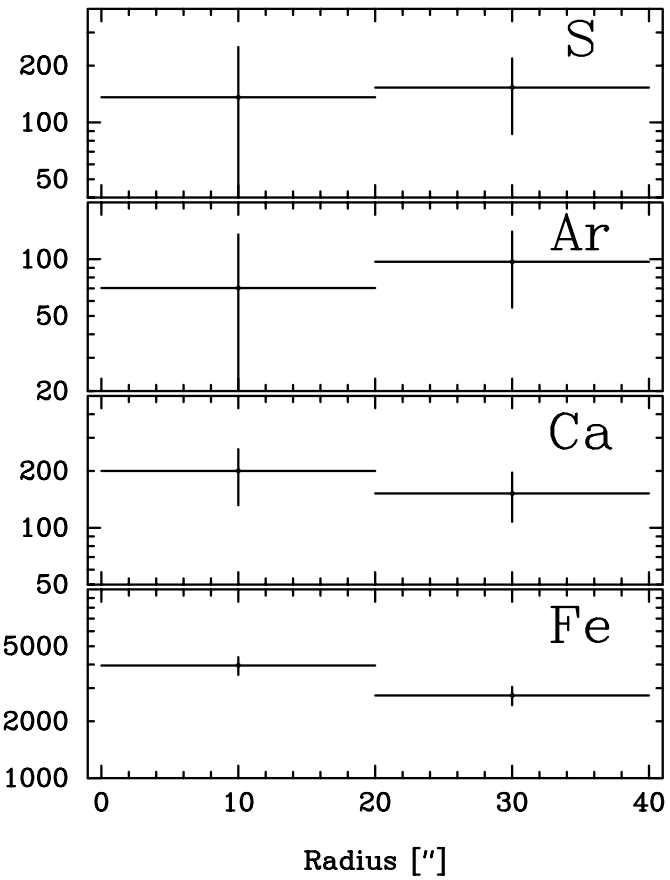

FIG. 7*b*

FIG. 7.—Plots of best-fit parameters for two concentric annuli. (*a*) Continuum. The units for $N_{\rm H}$ and kT_e are 10^{22} cm^{-2} and keV, respectively. (*b*) Equivalent widths for emission lines. The unit is eV. Note that the ordinates for both plots on (*b*) are logarithmic and span 1 order of magnitude.

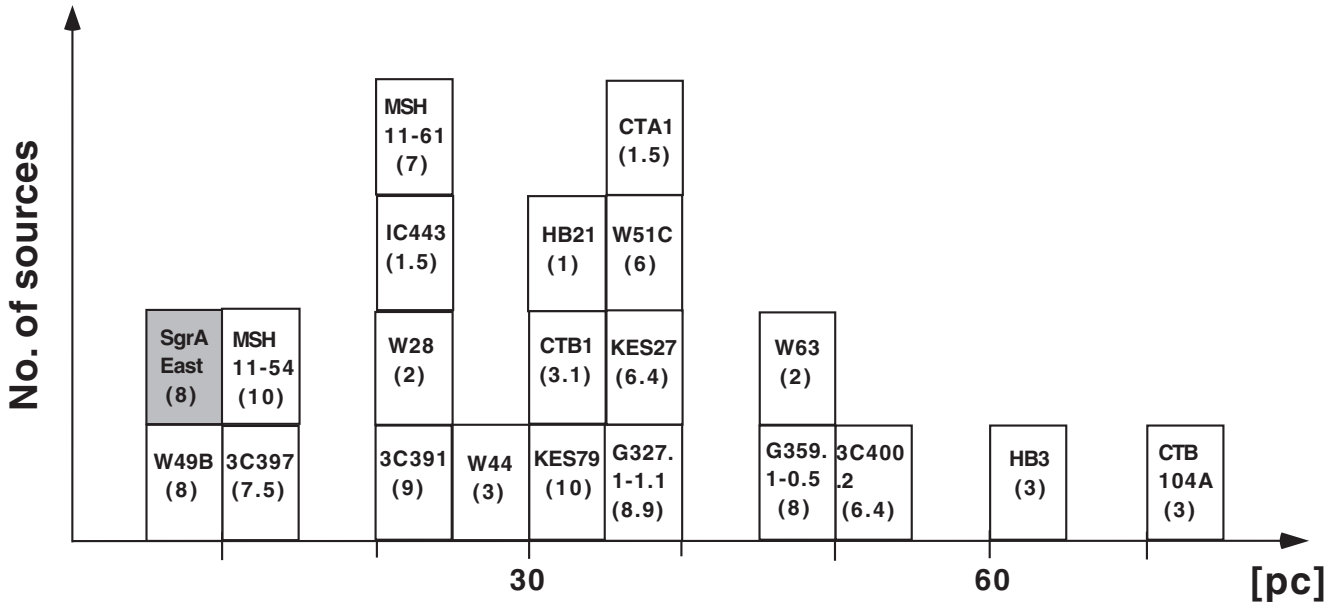

FIG. 8.—Histogram of the linear sizes of MM SNRs. Values given in parentheses are the assumed distances in kiloparsecs (see Rho & Petre 1998; Bamba et al. 2000 and references therein).

within a shell-like nonthermal radio structure. They called these objects "mixed morphology" (MM) supernova remnants and identified 19 members of the class. Bamba et al. (2000) reported that G359.1−0.5, which, like Sgr A East, is in the Galactic center region, shares the defining features of MM SNRs. With the centrally concentrated X-ray emission we find here and its well-established nonthermal radio shell, Sgr A East becomes a new member of the class of MM SNRs. Additional evidence for this conclusion is provided by the 1720 MHz OH masers present in the Sgr A East shell (Yusef-Zadeh et al. 1996). Such masers are often detected in MM SNRs (Green et al. 1997).

Figure 8 plots a histogram of MM SNR sizes including Sgr A East. No historical SNR, such as Tycho, is an MM-SNR, suggesting that Sgr A East is not very young with an age roughly $t > 10^3$ yr old. No MM SNRs are seen in the LMC or SMC, in which interstellar matter is known to be less dense than that of the Galaxy. Figure 8 shows that Sgr A East is the smallest of the MM SNRs, probably indicating Sgr A East is evolving into ambient materials denser than those for the usual MM SNRs. One MM SNR, W49B (G43.3−0.2), has a size similar to that of Sgr A East. The basic properties of Sgr A East and W49B are summarized in Table 3. The X-ray properties of W49B and Sgr A East are also similar (Pye et al. 1984; Smith et al. 1985; Fujimoto et al. 1995; Sun & Wang 2000; Hwang, Petre, & Hughes 2000): (1) the equivalent width of the iron K-line is very large, indicating a plasma enriched in heavy elements; (2) narrowband X-ray imaging indicates a spatial gradient of elemental abundance where the distribution of iron is more compact than those of the lighter elements; (3) X-ray spectra indicate an X-ray plasma in collisional ionization equilibrium. The

TABLE 3
COMPARISON BETWEEN SGR A EAST AND W49B

PARAMETER	OBSERVED QUANTITIES		REFERENCES	
	Sgr A East	W49B	Sgr A East	W49B
Distance (kpc)	8	8	1	2, 3
Radio (nonthermal)				
Morphology	Shell (ellipse)	Shell (roughly circular)	4	5
Size (arcmin)	3.5×2.5	3.5	4	5
Spectral index (ν^{α})	−0.8	−0.5	6	6
Flux at 1 GHz (Jy)	100	38	6	6
X-rays (optically thin thermal)				
Morphology	Centrally concentrated	Centrally concentrated	This work	5
kT_e (keV)	2	2	This work	7
$L_{2-6\ \mathrm{keV}}$ (ergs s^{-1})	6×10^{34}	6×10^{35}	This work	7
Equivalent width of Fe K (keV)	3	5	This work	7
Intensity of Fe K (photons cm^{-2} s^{-1})	1×10^{-4}	1×10^{-3}	This work	7

REFERENCES.—(1) Reid 1993; (2) Radhakrishnan et al. 1972; (3) Moffett & Reynolds 1994; (4) Ekers et al. 1975; (5) Pye et al. 1984; (6) Green 1991; (7) Smith et al. 1985.

close resemblance between W49B and Sgr A East confirms the notion that Sgr A East is best interpreted as an SNR and is not a unique object.

Exotic hypotheses invoking the nearby MBH, such as an explosion inside a molecular cloud possibly due to a tidally induced catastrophic event occurring $\sim 10^5$ yr ago within 10 Schwarzschild radii of the MBH (Yusef-Zadeh & Morris 1987; Khokhlov & Melia 1996), are not likely to reproduce the metal-rich plasma because the explosion is driven by gravity rather than by a nuclear reaction. The other exotic hypothesis—near-simultaneous explosions of $\sim$40 SNe (Mezger et al. 1989)—can produce heavy elements, but this hypothesis is very strongly constrained by the short expansion time of the shell and by the absence of a massive, young stellar cluster near the center of the shell. In summary, the most straightforward hypothesis for the origin of Sgr A East is a single supernova. Alternative hypotheses are hard pressed to quantitatively reproduce both the X-ray and radio properties.

4.2. *Age*

Mezger et al. (1989) estimated the age of Sgr A East to be $t \sim 7500$ yr, assuming that an SNR evolves into a bubble in a giant molecular cloud formed by a stellar wind from the progenitor. Uchida et al. (1998) independently derived an age of a few 10^4 yr based on the shear effect owing to the differential Galactic rotation. These ages are roughly close to that of W49B (10^3–10^4 yr; see Moffett & Reynolds 1994 and reference therein) and is consistent with that of a typical MM SNR ($t > 10^3$ yr). These arguments support an age of Sgr A East of approximately 10,000 yr. This age is also consistent with the observed X-ray properties as discussed in the later sections.

Note that the age is too short to form the compact H II regions that are probably 10^5–10^6 yr old seen in radio continuum maps (Fig. 3). We thus support the argument by Serabyn, Lacy, & Achtermann (1992) that Sgr A East did not stimulate star formation running along the chain of the compact H II regions.

4.3. *Plasma Diagnostics*

Since the electron density of the X-ray plasma is $\sim 6\eta^{-1/2}$ cm^{-3}, the ionization parameter ($n_e t \simeq 2 \times 10^{12}\eta^{1/2}$ cm^{-3} s assuming $t = 1 \times 10^4$ yr) is near the characteristic timescale for realizing collisional equilibrium (Masai 1994). For this density and temperature, the electrons and ions should reach energy equipartition in 10^3 yr (Spitzer 1962), which is an order of magnitude shorter than the age estimated for Sgr A East. The sound crossing length, an effective length for heat conduction, is $\sim$8 pc at 10^4 yr, which is longer than the radius of the plasma ($\sim$1.6 pc). The radiative cooling time of the plasma is 10^6 yr. Our phenomenological success in fitting an isothermal MEKA model (a single temperature plasma in collisional ionization equilibrium) to the spectrum (§ 3.2; Figs. 5 and 7) is completely consistent with those plasma conditions, which now have a physical foundation. Therefore, the total energy of the plasma derived by assuming energy equipartition, 10^{49} ergs, is likely to be correct.

4.4. *Stellar Progenitor*

Recall from § 3.2 that the best-fit relative abundance gives $z_{\rm Fe} = 1.1$ and that, averaged over the remnant, iron is as abundant as the other heavy elements. Type Ia explosions give the highest ejection of Fe/Ni–group elements ($z_{\rm Fe} \sim$ a few), while Type II explosions on average give lower abundances ($z_{\rm Fe} \simeq 0.5$; e.g., Tsujimoto et al. 1995). Among Type II explosions, the iron abundance is about unity for a progenitor mass of $M = 13$–$20\ M_\odot$ but is lower by an order of magnitude for $M = 40$–$70\ M_\odot$ (e.g., Nomoto et al. 1997). Therefore, the observed iron abundance corresponds to that predicted for a Type II explosion in a progenitor star of mass 13–20 $M_\odot$. A supernova from a progenitor in this mass range ejects 1–5 $M_\odot$ of material, which is consistent with the 2 $M_\odot$ of plasma deduced in § 3.2 assuming a high volume filling factor ($\eta \sim 1$). The explosion energy of this type of SN is 10^{51} ergs, which is 1 or 2 orders of magnitude smaller than the total energy suggested by Mezger et al. (1989).

A Type II explosion is believed to produce a neutron star that is often kicked up to a fairly high velocity (for a fast case, $\sim$700 km s^{-1}; Cordes & Chernoff 1998). The kicked neutron star might thus have traveled a distance of 700 km s^{-1} $\times$ 10^4 yr = 7 pc. Since the ambient material is dense (§ 4.5), the neutron star running through it could produce a strong bow shock, which might account for the observed linear X-ray feature, the "plume." The distance traveled is, in projection, about $3' \times \sin\theta$, where θ is the angle between the neutron star's motion and the line of sight. The observed linear feature, with a length of $\sim 0\farcm5$, could be consistent with a bow shock tail of the neutron star if its velocity vector is close to the line of sight. A future *Chandra* observation with a very long exposure would probably be the best way to determine whether a neutron star is present at the tip of the plume.

4.5. *Dynamical Evolution I: Forward Shock and Ambient Environment*

Two scenarios have been put forth to explain the formation of MM SNRs: cloud evaporation or "fossil radiation." In the evaporation scenario, the enhanced interior X-ray emission arises from gas evaporated from cold interstellar clouds that were enveloped by the SNR (White & Long 1991). Clouds too small to upset the overall forward-shock propagation and of sufficient density to survive passage through the shock provide a reservoir of material inside the remnant cavity. Their subsequent evaporation increases the density of the hot interior and hence the X-ray emissivity. The clouds must be numerous and have a small filling factor in order to produce the X-ray emission without affecting the shock dynamics. In the fossil radiation scenario, the SNR moves into a dense and less clumpy ISM that is almost completely snowplowed into a dense shell by the advancing shock (McKee & Cowie 1975). The SNR has a luminous plasma shell associated with the forward shock, but this shell has cooled to low temperatures that would be undetectable in X-rays through the line-of-sight absorbing material toward the Galactic center. The presence of this shell is instead revealed by radio emission. The ejecta heated by the reverse shock is thus detected as "fossil" thermal radiation within an invisible shell (McKee 1974). Here the X-ray–emitting plasma is dominated by the ejecta, whereas it is dominated by ordinary interstellar material in the cloud formation scenario. The highly metal-enriched spectrum found in Sgr A East favors the fossil radiation scenario, i.e., ejection into a dense and homogeneous ambient environment.

Mezger et al. (1989) and Uchida et al. (1998) have already discussed the dynamical evolution of the Sgr A East SNR on the basis of its radio properties. The picture of the ambient material given by Mezger et al. (1989) is that of a huge wind bubble formed in a giant molecular cloud, while Uchida et al. (1998) consider a less dense and homogeneous gas. The X-ray properties then support the picture of Uchida et al. (1998). Sgr A East is likely to be in the region of non–solid-body rotation near the gravitational center, Sgr A* (e.g., Uchida et al. 1998), where the rotation timescale is $\sim 4 \times 10^4 (R/1 \text{ pc})^{1.5}$ yr at Galactrocentric radius R (see rotation curve in Lugten et al. 1986). Differential rotation tends to shear the ISM and to smooth it out in a few rotation cycles ($\sim 10^5$ yr). These considerations favor the homogeneous ambient environment.

The nonthermal radio emission from Sgr A East in the direction of Sgr A West is very faint, mainly because of the heavy absorption by the spiral-shaped group of thermal gas streams called the minispiral (Yusef-Zadeh & Morris 1987; Pedlar et al. 1989; Anantharamaiah et al. 1999). These authors also reported that a turnover (absorption) occurs at 90 cm from both Sgr A East and West, which suggests the presence of an ionized gas halo extending over the Sgr A complex. This ionized halo has an implied emission measure of $\sim 10^5$ pc cm^{-6} and an optical depth at 90 cm of around unity. Anantharamaiah et al. further suggest that it has an angular extent of $\sim 4'$ (~ 9 pc), an electron density of 10^2–10^3 cm^{-3}, and an electron temperature of maybe 0.5–1 eV. The radial extent of the ionized gas halo nearly corresponds to that of the non–solid-body rotating region (~ 10 pc). Therefore, the most straightforward idea is that an ionized gas halo is filling the non–solid-body rotation region with a nearly homogeneous density, and that Sgr A East is expanding into this ionized gas halo (Fig. 9).

Another potential candidate for the ambient material is the "diffuse X-ray plasma," which extends across the inner few hundred parsecs of the Galactic center (Koyama et al. 1989). The temperature of the diffuse X-ray plasma is as high as 10 keV, so the Mach number is probably less than unity and the SNR will expand without interaction. This is likely to be inconsistent with the existence of the forward shock evidenced by the bright radio shell (Fig. 3). This argument is also consistent with the alternative interpretation for the diffuse X-ray emission—that the emission does not originate from a thin thermal plasma but is due to charge-exchange interactions of low-energy cosmic-ray heavy ions (Tanaka et al. 2000).

The dynamical evolution of Sgr A East in the Galactic latitudinal direction (perpendicular to the plane) might not be affected by Galactic rotation or by the strong and perhaps vertical magnetic fields (Morris & Serabyn 1996 and references therein), so we can directly compare the latitudinal extent of Sgr A East to that predicted by the simple theory for dynamical evolution of an SNR (Lozinskaya 1992). The

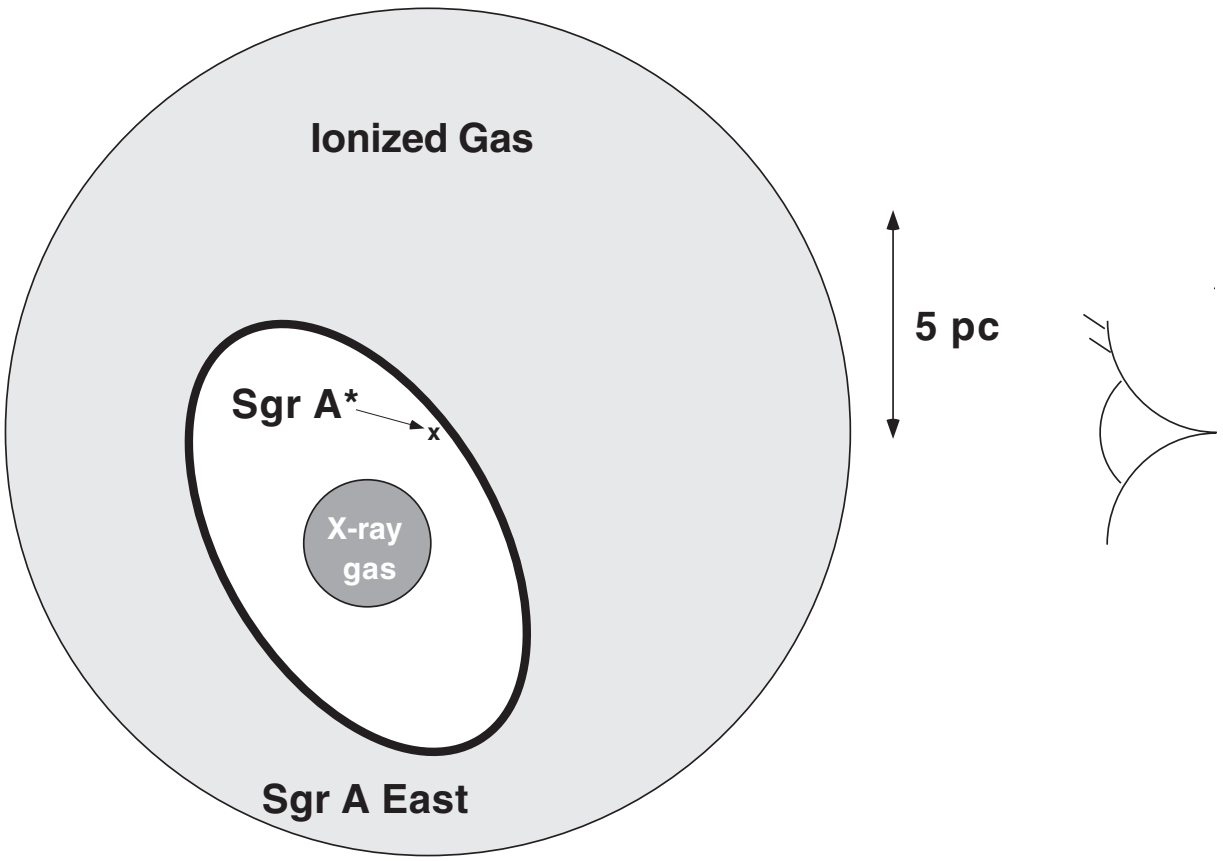

FIG. 9.—Schematic diagram of the relative positions and sizes of Sgr A*, Sgr A East, and the ionized gas halo along the line of sight from the Sun with the positive Galactic longitude (east) at the bottom. The ionized gas halo of 10^3 cm^{-3} is rotating around Sgr A* and is filling the non–solid-body rotation region. An SNR, Sgr A East, was expanding into the ionized gas halo, and the radio structure associated with the slow forward shock was sheared by the Galactic rotation. The hot ejecta plasma is centrally concentrated within the Sgr A East radio shell and is visible in X-rays. Sgr A* was hit by the front edge of the Sgr A East shell in the recent past and is currently in the hot cavity inside of the shell.

theory predicts that, at an age of 10^4 yr, Sgr A East is presently in its radiative phase. Although the dynamical evolution in the radiative phase of the theory is somewhat uncertain, the radius is predicted to be 6 $(t/10^4 \text{ yr})^{0.31}$ $(n_e/10^3 \text{ cm}^{-3})^{0.25}$ pc, where the total mass, the initial velocity of the ejecta, and elemental abundances are assumed to be 2 $M_\odot$, 10^4 km s^{-1}, and solar, respectively. If the electron density n_e of the ambient gas is 10^3 cm^{-3}, corresponding to the denser estimate for the ionized gas halo, the radius roughly agrees with that of the radio shell ($\sim$2.9 pc; see Fig. 3). The large column density of the ionized gas halo, 3×10^{22} H cm^{-2} $(R/10 \text{ pc})$ $(n_e/10^3 \text{ cm}^{-3})$, is presumably related to the observed discrepancy between the optical extinction to the GC ($A_V \simeq 30$ mag or $N_{\rm H} \simeq 5 \times 10^{22}$ cm^{-2}) and the X-ray absorption column density ($N_{\rm H} \simeq 10 \times 10^{22}$ H cm^{-2}), as discussed in Paper I. The discrepancy can be explained if the ratio of dust grains to atoms is much smaller in the ionized gas halo than in the foreground gas; infrared light is extinct mainly by the foreground gas, while X-rays are absorbed by both the foreground and the ionized halo gas around Sgr A East.

Lozinskaya predicts the shock velocity for the blast wave to be as slow as 2×10^2 $(t/10^4 \text{ yr})^{-0.69}$ km s^{-1} and that the postshock temperature is as warm as $\sim$70 eV. Ultraviolet and soft X-rays from the warm plasma should be completely absorbed, which is consistent with the nondetection of X-rays from the radio shell. The cooling time of the warm plasma is shorter than 1 yr (Raymond & Smith 1977), which is at least 4 orders of magnitude shorter than the SNR age. The rapid cooling implies a cooled thermal shell in the forward shock region. In fact, the cooled thermal shell was detected as a dust ridge surrounding the nonthermal radio shell by Mezger et al. (1989; see Fig. 1).

Mezger et al. also found that the dust ridge in the eastern half is so dense that molecular line emission is detectable; thus it is called the curved molecular ridge (hereafter "the molecular ridge"). They found that the total gas mass of the dust/molecular ridge was 6×10^4 $M_\odot$. With the assumption of a high filling factor, $\sim$1, the total gas mass of the molecular ridge was independently derived as 1.5×10^5 $M_\odot$ using the molecular-line observations (Coil & Ho 2000 and references therein). This is 20–50 times larger than the mass of $3 \times 10^3 (r_{\rm SNR}/2.9 \text{ pc})^3$ $M_\odot$ that the Sgr A East shell is able to accumulate from the ambient matter having $n_e = 10^3$ cm^{-3}.

The mass discrepancy reminds us of the arguments by Mezger et al. (1989; see also Yusef-Zadeh et al. 2000 and reference therein) that the eastern part of Sgr A East has been expanding into the +50 km s^{-1} cloud, sweeping up gas at the western edge of the cloud, compressing it, and forming a substantially denser ridge at the eastern edge of Sgr A East than on the western side (see Fig. 1). In this case, the compressed gas mass is mostly included in the western shell, the mass of which becomes $\sim 10^5$ $M_\odot$ because the density of the +50 km s^{-1} cloud (10^5 cm^{-3}) is about a 100 times higher than that of the ionized gas halo (Coil & Ho 2000). The mass of 10^5 $M_\odot$ is consistent with the mass presently surrounding the shell. The cloud should also brake the eastern shell of Sgr A East, the speed of which is reduced by a factor of 10 to $\sim$20 km s^{-1}). The small velocity dispersion of the molecular ridge (a few $\times$ 10 km s^{-1}; Coil & Ho 2000) is highly consistent with this picture.

As the eastern side of the Sgr A East shell should be located farther away from the gravitational center at Sgr A* than the western side, and the Galactic rotation timescale is proportional to $\sim 1/R^{1.5}$, the large +50 km s^{-1} cloud can probably persist for as long as 10^6 yr before being sheared so much that it becomes a continuous stream of gas rather than a well-defined cloud. We therefore propose a picture in which most of the Sgr A East shell is expanding into the ionized gas halo where the density is $\sim 10^3$ cm^{-3}, but the eastern side has encountered the much denser +50 km s^{-1} molecular cloud. The implication of this model is that the expansion has proceeded farther toward the west than toward the east.

While the thermalized component associated with the shock front experiences large radiative cooling by atomic processes, the nonthermal component observed as a nonthermal radio shell should lose a large amount of energy by the synchrotron process operating in the strong milligauss magnetic field. The nondetection of X-rays from the radio shell and the steep synchrotron radio spectrum are both understood simply in terms of radiative energy loss (Pedlar et al. 1989). Melia, Yusef-Zadeh, & Fatuzzo (1998) suggested the possibility that infrared light from Sgr A West might be Comptonized within the radio shell to the hard X-ray band with a fairly high luminosity of $L_{\rm X} \simeq 2 \times 10^{35}$ ergs s^{-1}. This is at least 2 orders of magnitude higher than the observed X-ray emission from the radio shell, so this model is apparently not applicable.

4.6. *Dynamical Evolution II: Reverse Shock and SN Ejecta*

The interaction of the forward shock with the dense surrounding medium will have produced a reverse shock propagating back into the expanding ejecta. Since the electron temperature of the X-ray plasma is $\sim$2 keV, we expect the shock velocity v_s to be $\sim$1000 km s^{-1}, which is about 5 times faster than the present shock velocity expected for the forward shock ($\sim$200 km s^{-1}; see § 4.5). This discrepancy indicates that the reverse shock has already propagated back through the bulk of the X-ray–emitting plasma, and the high velocity suggests that the reverse shock has already arrived at the center in an early phase and that the ejecta have been thermalized.

In SN explosions predicted by standard nucleosythesis theories, the lighter elements like S, Ar, and Ca are expected to be ejected faster than Fe (e.g., Nomoto et al. 1997). If mixing is not effective, the stratification of the elements may show up in the ejecta plasma. In Figure 4, we saw that the spatial extent in the 6–7 keV band is smaller than those in the lower energy bands. The spectrum in Figure 5 shows that the flux from the iron K-lines dominates the 6–7 keV band, while the sulphur and calcium lines enhance the 1.5–3 and 3–6 keV bands, respectively. The energy dependence of the spatial extent suggests that the heaviest elements are more compactly distributed than the lighter ones. The spatial distribution in every energy band shows a centrally concentrated morphology (Fig. 2), which indicates that the elements coexist at the inner region. The coexistence can be simply explained if the elements in the supernova ejecta are not perfectly stratified and well mixed in the inner region.

The velocity dispersion of the 2 keV plasma is $\sim$620 $(1/A)^{1/2}$ km s^{-1}, where A is the atomic mass. So the mixing length is estimated to be $\sim$6.3 $(1/A)^{1/2}$ $(t/10^4 \text{ yr})$ pc, with which we can estimate the mixing angular scale on the sky of ^{32}S and ^{56}Fe to be 29″ and 22″, respectively. These values are very similar to the observed scale radii of $\sim$30″ and

$\sim 20''$ in the 1.5–3 and 6–7 keV bands. Hence, the estimated age of 10,000 yr is long enough for the light materials, like S, to reach the center but is too short for iron to reach the outward light elements layer. The observed spatial gradient of elements could be consistent with the elemental stratification predicted by standard nucleosythesis theories if significant mixing occurs after the ejecta were thermalized.

The observed brightness of the X-ray emission is centrally concentrated, indicating that the outer region of the ejecta plasma is sparse. In fact, as the forward shock compresses the ambient materials, a hot cavity is expected to be formed inside of the forward shock layer (Chevalier 1982). The ejecta plasma seen in X-rays might currently be undergoing mixing as well as diffusing into the hot cavity.

4.7. *The Ionized Gas Halo and Its Irradiating Source*

The radio nonthermal shell still exists, indicating that the forward shock velocity of the shell is faster than the sound velocity of the ambient material, "the ionized gas halo." Therefore, the temperature of the ionized gas halo is substantially lower than ~ 70 eV. If the halo is collisionally ionized, the temperature should be higher than ~ 10 eV. The radiative efficiency is known to have a peak around 20 eV. So in order to keep the temperature in the range between 10 and 70 eV, kinematic heating of 10^{43} $(n_e/10^3\ \mathrm{cm}^{-3})$ $(R/10\ \mathrm{pc})^3$ ergs s^{-1} is required. Such an energetic source cannot be found in the Galactic center region, so the gas should have rapidly cooled down in 1 yr, which argues strongly against collisional ionization heating.

An alternative is that photoionization ionizes the gas halo, in which case the kinematic temperature is much lower than 10 eV. Since the column density is 3×10^{22} H cm^{-2} $(R/10\ \mathrm{pc})$ $(n_e/10^3\ \mathrm{cm}^{-3})$, ultraviolet photons can contribute the ionization of only a local and small portion of the ionized gas halo. X-rays above ~ 1 keV are expected to be the main contributor to photoionization. Although the photoionization cross is highly dependent on the spectral slope of the irradiating X-ray source, $L_{\mathrm{X}} \simeq 10^{40}(n_e/10^3\ \mathrm{cm}^{-3})(R/10\ \mathrm{pc})$ is required to ionize most of the hydrogen atoms in the non–solid-body rotation region (see Kallman & McCray 1982, Fig. 3). However, no persistent X-ray source brighter than an order of 10^{36} ergs s^{-1} is located in the Galactic center region (e.g., Pavlinsky, Grebenev, & Sunyaev 1994).

The absence of a predicted bright X-ray irradiator reminds us of the study of Sgr B2, a unique X-ray reflection nebula near the Galactic center (Koyama et al. 1996; Murakami et al. 2000). They found fluorescent X-ray emission from cold iron atoms in molecular clouds, possibly owing to irradiation by X-rays from Sgr A*, which was bright 10^3 yr ago but is presently dim. By applying a detailed model of an X-ray reflection nebula to the Sgr B2 molecular cloud, they estimated the X-ray luminosity of Sgr A* 300 yr ago to be $\sim 3 \times 10^{39}$ ergs s^{-1}, which is comparable with that required to ionize the gas halo ($\sim 10^{40}$ ergs s^{-1}). The recombination time in a 10^3 cm^{-3} gas is as short as ~ 300 yr. Thus, the high-ionization fraction in the ISM rotating in the non–solid-body rotation region could be due to the past activity of Sgr A* at about 10^2–10^3 yr ago and the ISM is presently in a recombination-dominated phase. Thus, the existence of the ionized gas halo surrounding Sgr A* supports the scenario that Sgr A* experienced active galactic nucleus (AGN) activity in the recent past (Sunyaev, Markevitch, & Pavlinsky 1993; Koyama et al. 1996; Murakami et al. 2000, 2001). Note that the gas halo would have been neutral before the recent AGN activity if no other irradiator was present.

4.8. *Comments on a Possible Relation between Sgr A East and Sgr A**

The nonthermal radio emission from Sgr A East in the direction of Sgr A West is heavily absorbed by Sgr A West (Yusef-Zadeh & Morris 1987; Pedlar et al. 1989). This fact convincingly indicates that, along the line of sight, Sgr A West lies in front of the Sgr A East shell. However, the distance between Sgr A West and Sgr A East along the line of sight is uncertain. It is quite possible that they lie at nearly identical distances, in which case the front edge of the expanding Sgr A East shell has probably reached and passed through Sgr A West (Morris & Serabyn 1996 and reference therein). This configuration is simply illustrated in Figure 9 (see Yusef-Zadeh et al. 2000 for a more thorough discussion).

Four observations support this hypothesis. First, if a structure of size much smaller than the scale of Sgr A East is being overrun by the forward shock of the SNR, a bow shock should form in the direction of explosion of Sgr A East (McKee & Cowie 1975). Such features may have been found from the molecular ring in recent radio studies (Yusef-Zadeh et al. 2000). Second, if Sgr A West is embedded within the nonthermal shell of Sgr A East, the radio emission from the front side of the nonthermal shell could escape being absorbed by the thermal ionized gas in Sgr A West. Yusef-Zadeh et al. (2000) report that there is indeed faint, nonthermal emission present toward the thermal ionized gas at 90 cm. Third, if Sgr A East is located very near Sgr A*, it should be sheared by the nonsolid Galactic rotation (Uchida et al. 1998). Yusef-Zadeh et al. (1999) reported that the kinematics of the OH maser spots associated with Sgr A East are consistent with such shear motions and with a separation less than 5 pc. Fourth, we found that, except for the $+50$ km s^{-1} molecular cloud, the ambient matter surrounding Sgr A East was probably homogeneous, giving rise to the dust ridge that appears all around the shell. However, the dust ridge surrounding most of Sgr A East (Fig. 1) is likely to be missing in the vicinity of Sgr A West (Mezger et al. 1989; Dent et al. 1993). This discrepancy suggests that the dust ridge has overrun Sgr A West and has been dynamically disrupted there by merging with the circumnuclear disk or, to a lesser extent, by accretion onto the MBH at Sgr A*. It is thus likely that Sgr A* lies within "the hot cavity" inside the matter compressed by the shock front. The radio image in projection is consistent with this scenario (Fig. 1). However, it is less obvious that Sgr A* is in direct contact with the hot medium within the shell because of competition from the winds emanating from the massive emission-line stars in the central cluster (see Paper I).

Assuming that the dynamical force of stellar winds in the central parsec is negligible, then, using the Bondi-Hoyle theory (Bondi & Hoyle 1944) we can roughly estimate the expected accretion rate of gas onto the MBH as the dust ridge compressed by the SNR shock passes Sgr A*. When the dust ridge passes by, the radius within which material falls onto the MBH with a mass of M_{MBH} is regulated prin-

cipally by the velocity of the dust ridge, $v_{\rm dust}$, according to

$$R_{\rm Bondi} = 0.5 \text{ pc} \left(\frac{v_{\rm dust}}{200 \text{ km s}^{-1}}\right)^{-2} \left(\frac{M_{\rm MBH}}{2.6 \times 10^6 \ M_\odot}\right) \quad (1)$$

with a corresponding accretion rate

$$\dot{M}_{\rm bondi} = 0.02 \ M_\odot \text{ yr}^{-1} \left(\frac{n_{\rm dust}}{4000 \text{ cm}^{-3}}\right) \left(\frac{v_{\rm dust}}{200 \text{ km s}^{-1}}\right)^{-3} \times \left(\frac{M_{\rm MBH}}{2.6 \times 10^6 \ M_\odot}\right)^2, \quad (2)$$

where $n_{\rm dust}$ is the mean electron density assuming that the ambient material of 10^3 cm^{-3} is compressed by a factor of 4, and $v_{\rm dust}$ is the expanding velocity of the dust ridge assuming the same as the shock velocity expected for the forward shock. The crossing time of the dust shell is

$$t_{\rm crossing} \simeq 1 \times 10^3 \text{ yr} \left(\frac{\Delta \rm R}{0.24 \text{ pc}}\right) \left(\frac{v_{\rm dust}}{200 \text{ km s}^{-1}}\right)^{-1}, \quad (3)$$

where ΔR is the width of the dust ridge assuming 1/12 of the radius of the ridge. The total accreted mass is roughly estimated to be 20 $M_\odot (R_{\rm bondi}/0.5 \text{ pc})^2$. The predicted mass accretion of around 10^{-2} $M_\odot$ yr^{-1} is comparable to the Eddington limit of 5×10^{-3} $M_\odot$ yr^{-1}, suggesting Sgr A* could have been as bright as the Eddington luminosity of 3.4×10^{44} ergs s^{-1} for $\sim 1 \times 10^3$ yr. Hence, the dust ridge, the ISM compressed by the forward shock of Sgr A East, might be dense enough to activate the massive black hole to Seyfert or quasar luminosity level in the recent past.

It is possible, however, that stellar winds might impede the accretion of the dust ridge. The winds from the central cluster of early-type emission-line stars have an estimated integrated mass loss rate $\dot{M}_{\rm winds} \simeq 4 \times 10^{-3}$ $M_\odot$ yr^{-1} with an average wind velocity $v_{\rm winds} \simeq 700$ km s^{-1}, inferred from hydrogen Brγ line observations (Yusef-Zadeh et al. 2000). At a distance of half a parsec, roughly the size of the stellar cluster, the ram pressure from the winds

$$\rho_{\rm winds} v_{\rm winds}^2 \simeq 1 \times 10^{-6} \text{ dynes cm}^{-2} \quad (4)$$

is comparable to the estimated ram pressure of the dust ridge,

$$\rho_{\rm dust} v_{\rm dust}^2 \simeq 3 \times 10^{-6} \text{ dynes cm}^{-2} \left(\frac{n_{\rm dust}}{4 \times 10^3 \text{ cm}^{-3}}\right) \times \left(\frac{v_{\rm dust}}{200 \text{ km s}^{-1}}\right)^2. \quad (5)$$

The stellar winds could thus impede the captured dust ridge from accreting onto the MBH. The accretion rate would then be reduced by an unknown factor.

We suggest that the dense dust ridge arrived near the MBH and its surrounding central cluster about (1–2) $\times 10^3$ yr ago, producing an increased external ram pressure that overwhelmed the pressure of the stellar winds which led to a large jump in the accretion rate, triggering the AGN activity that ionized the gas halo around Sgr A East and is illuminating the more distant molecular cloud Sgr B2. The ridge passed by the MBH 100 or 200 yr ago and the luminous X-rays associated with the AGN activity faded away. The accretion from the dust ridge was completely finished before the beginning of X-ray astronomy and the MBH at Sgr A* has never been detected in X-rays before the *Chandra* era (Paper I; Maeda et al. 1996 for a history of X-ray observations). Sgr A* is then currently embedded in the hot cavity of the Sgr A East SNR, in which little accretion is possible and the MBH is observed in a very quiescent state with $L_{\rm X} \simeq 10^{33}$ ergs s^{-1} (Paper I).

5. CONCLUSION AND SUMMARY

Using the ACIS instrument on board *Chandra*, we have spatially resolved for the first time the X-ray emission of the shell-like nonthermal radio source Sgr A East (SNR 000.0+00.0) from the other complex X-ray structures present in the Galactic center. We find the X-ray emission is concentrated within the central $\simeq$2 pc radius of the larger $\sim$6–9 pc radio shell. The spectrum clearly originates within an optically thin thermal plasma with strong Kα lines from highly ionized heavy atoms, indicating an overabundance of heavy elements several fold above solar levels. The elemental abundances show a spatial gradient: the distribution of iron is more compact than the lighter elements. The morphology (mixed morphology), energetics ($\sim 2 \times 10^{49}$ $\eta^{1/2}$ ergs s^{-1}), and mass ($2\eta^{-1/2}$ $M_\odot$) are all consistent with a single supernova remnant origin. The relative abundances between heavy elements favors Sgr A East originating from a Type II SN of a 13–20 $M_\odot$ progenitor star. An exotic origin related to the Sgr A* massive black hole is not required.

While detailed modeling of the structure is subject to considerable uncertainties, we have evaluated a simplified model for the dynamical evolution of Sgr A East as an SNR formed about 10,000 yr ago by a Type II supernova. In this model, the ejecta expanded into a homogeneous and dense interstellar medium of 10^3 cm^{-3} that pervades the central $\sim$10 pc around the Galactic center. We see the SNR today when the forward shock is relatively slow, explaining the absence of hard X-rays associated with the larger radio shell. The reverse shock was relatively fast, forming a hot plasma in the interior of the remnant that is still visible in the hard X-ray band. The result is a rare subtype of SNR: a very compact "mixed morphology" remnant. Of all known SNRs, only W49B appears to be similar to Sgr A East.

Sgr A East is interacting with the +50 km s^{-1} molecular cloud on its eastern side. Its relationship to Sgr A West is still controversial. We suggest that the dust ridge compressed by the forward shock reached Sgr A* $\sim 10^3$ yr ago. The passage of the dust ridge may have led to increased accretion onto the MBH and triggered nuclear activity, the remains of which are observed today as the ionized gas halo surrounding Sgr A* with a radial extent of $\sim$9 pc and the X-ray reflection nebula, seen in the more distant Sgr B2 molecular cloud. The MBH at Sgr A* might currently lie within the hot cavity of the Sgr A East SNR and is thus starved of accreting material, explaining the extremely low X-ray luminosity from Sgr A* reported in Paper I. Thus, the Galactic center might be a laboratory in which a single supernova remnant has controlled the activity of the nuclear MBH. This could be a realization of the broad concepts relating nuclear starburst to MBH accretion activity in galactic nuclei (e.g., Heckman 2000).

This observation was performed as part of the guaranteed time observation (GTO) program awarded to the ACIS development team led by Gordon Garmire. We express our thanks to the entire *Chandra* team for their many efforts in

fabricating, launching, and operating the satellite, and for their work in developing software for calibrating and analyzing the data. Rashid Sunyaev shared valuable thoughts with us on Galactic center issues. Steven Reynolds, Jack Hughes, and other attendees of the 11th Maryland conference "Young Supernova Remnants" honoring the retirement of Steve Holt, kindly elucidated SNR astrophysics. Farhad Yusef-Zadeh and his collaborators kindly provided us with an unpublished radio image, and the ACIS Hubble Deep Field team gave us access to their data for calibration purposes. This research was supported by NASA contract NAS 8-38252 and in part (S. H. P.) by JPL, under contract with NASA. Y. M. was financially supported by the Japan Society for the Promotion of Science (JSPS).

REFERENCES

Anantharamaiah, K. R., Pedlar, A., & Goss, W. M. 1999, in ASP Conf. Ser. 186, The Central Parsecs of the Galaxy, ed. H. Falcke et al. (San Francisco: ASP), 422
Anders, E., & Grevesse, N. 1989, Geochim. Cosmochim. Acta, 53, 197
Baganoff, F., et al. 2001, ApJ, submitted (astro-ph/0102151) (Paper I)
Bamba, A., Yokogawa, J., Sakano, M., & Koyama, K. 2000, PASJ, 52, 259
Bondi, H., & Hoyle, F. 1944, MNRAS, 104, 273
Case, G. L., & Bhattacharya, D. 1998, ApJ, 504, 761
Chevalier, R. A. 1982, ApJ, 258, 790
Coil, A. L., & Ho, P. T. P. 2000, ApJ, 533, 245
Cordes, J. M., & Chernoff, D. F. 1998, ApJ, 505, 315
Cotera, A. S., Simpson, J. P., Erickson, E. F., Colgan, S. W. J., Burton, M. G., & Allen, D. A. 1999, ApJ, 510, 747
Dent, W. R. F., Matthews, H. E., Wade, R., & Duncan, W. D. 1993, ApJ, 410, 650
Ebeling, H., White, D., & Rangarajan, V. 2002, MNRAS, submitted
Ekers, R. D., Goss, W. M., & Schwarz, U. J. 1975, A&A, 43, 159
Ekers, R. D., van Gorkom, J. H., Schwarz, U. J., & Goss, W. M. 1983, A&A, 122, 143
Freeman, P. E., Kashyap, V., Rosner, R., & Lamb, D. Q. 2002, ApJS, 138, 185
Fujimoto, R., et al. 1995, PASJ, 47, L31
Goss, W. M., Schwarz, U. J., van Gorkom, J. H., & Ekers, R. D. 1985, MNRAS, 215, 69
Green, A. J., Frail, D. A., Goss, W. M., & Otrupcek, R. 1997, AJ, 114, 2058
Green, D. A. 1984, MNRAS, 209, 449
———. 1991, PASP, 103, 209
Heckman, T. M. 2000, Philos. Trans. R. Soc. London, 358, 2077
Ho, P. T. P., Jackson, J. M., Barrett, A. H., & Armstrong, J. T. 1985, ApJ, 288, 575
Hwang, U., Petre, R., & Hughes, J. P. 2000, ApJ, 532, 970
Jones, T. W. 1974, A&A, 30, 37
Kallman, T. R., & McCray, R. 1982, ApJS, 50, 263
Khokhlov, A., & Melia, F. 1996, ApJ, 457, L61
Koyama, K., Awaki, H., Kunieda, H., Takano, S., Tawara, Y., Yamauchi, S., Hatsukade, I., & Nagase, F. 1989, Nature, 339, 603
Koyama, K., Maeda, Y., Sonobe, T., Takeshima, T., Tanaka, Y., & Yamauchi, S. 1996, PASJ, 48, 249
Lozinskaya, T. A. 1992, Supernovae and Stellar Wind in the Interstellar Medium (New York: AIP)
Lugten, J. B., Genzel, R., Crawford, M. K., & Townes, C. H. 1986, ApJ, 306, 691
Maeda, Y., Koyama, K., Sakano, M., Takeshima, Y., & Yamauchi, S. 1996, PASJ, 48, 417
Masai, K. 1994, ApJ, 437, 770
McKee, C. F. 1974, ApJ, 188, 335
McKee, C. F., & Cowie, L. L. 1975, ApJ, 195, 715
Melia, F., Yusef-Zadeh, F., & Fatuzzo, M. 1998, ApJ, 508, 676
Mewe, R., Gronenschild, E. H. B. M., & van den Oord, G. H. J. 1985, A&AS, 62, 197
Mezger, P. G., Zylka, R., Salter, C. J., Wink, J. E., Chini, R., Kreysa, E., & Tuffs, R. 1989, A&A, 209, 337
Moffett, D. A., & Reynolds, S. P. 1994, ApJ, 437, 705
Morris, M., & Serabyn, E. 1996, ARA&A, 34, 645
Murakami, H., Koyama, K., Sakano, M., Tsujimoto, M., & Maeda, Y. 2000, ApJ, 534, 283
Murakami, H., Koyama, K., Tsujimoto, M., Maeda, Y., & Sakano, M. 2001, ApJ, 550, 297
Nomoto, K., Iwamoto, K., Nakasato, N., Thielemann, F. -K., Brachwitz, F., Tsujimoto, T., Kubo, Y., & Kishimoto, N. 1997, Nucl. Phys. A, 621, 467
Novak, G., Dotson, J. L., Dowell, C. D., Hildebrand, R. H., Renbarger, T., & Schleuning, D. A. 2000, ApJ, 529, 241
Pavlinsky, M. N., Grebenev, S. A., & Sunyaev, R. A. 1994, ApJ, 425, 110
Pedlar, A., Anantharamaiah, K. R., Ekers, R. D., Goss, W. M., van Gorkom, J. H., Schwarz, U. J., & Zhao, J. 1989, ApJ, 342, 769
Predehl, P., & Schmitt, J. H. M. M. 1995, A&A, 293, 889
Predehl, P., & Trümper, T. 1994, A&A, 290, L29
Prigozhin, G. Y., Kissel, S. E., Bautz, M. W., Grant, C., LaMarr, B., Foster, R. F., Ricker, G. R., & Garmire, G. P. 2000, Proc. SPIE, 4012, 720
Pye, J. P., Thomas, N., Becker, R. H., & Seward, F. D. 1984, MNRAS, 207, 649
Radhakrishnan, V., Goss, W. M., Murray, J. D., & Brooks, J. W. 1972, ApJS, 24, 49
Raymond, J. C., & Smith, B. W. 1977, ApJS, 35, 419
Reid, M. J. 1993, ARA&A, 31, 345
Rho, J., & Petre, R. 1998, ApJ, 503, L167
Serabyn, E., Lacy, J. H., & Achtermann, J. M. 1992, ApJ, 395, 166
Sidoli, L., & Mereghetti, S. 1999, A&A, 349, L49
Sidoli, L., Mereghetti, S., Israel, G. L., Chiappetti, L., Treves, A., & Orlandini, M. 1999, ApJ, 525, 215
Smith, A., Peacock, A., Jones, L. R., & Pye, J. P. 1985, ApJ, 296, 469
Spitzer, L. 1962, Physics of Fully Ionized Gases (New York: Wiley Interscience)
Sturner, S. J., Skibo, J. G., Dermer, C. D., & Mattox, J. R. 1997, ApJ, 490, 619
Sun, M., & Wang, Z. R. 2000, Adv. Space Res., 25, 549
Sunyaev, R. A., Markevitch, M., & Pavlinsky, M. 1993, ApJ, 407, 606
Tanaka, Y., Koyama, K., Maeda, Y., & Sonobe, T. 2000, PASJ, 52, L25
Townsley, L. K., Broos, P. S., Garmire, G. P., & Nousek, J. A. 2000, ApJ, 534, L139
Tsujimoto, T., Nomoto, K., Yoshii, Y., Hashimoto, M., Yanagida, S., & Thielemann, F.-K. 1995, MNRAS, 277, 945
Uchida, K. I., Morris, M., Serabyn, E., Fong, D., & Meseroll, T. 1998, in IAU Symp. 184, The Central Regions of the Galaxy and Galaxies, ed. Y. Sofue (Dordrecht: Kluwer), 317
Weisskopf, M. C., O'dell, S., & van Speybroeck, L. P. 1996, Proc. SPIE, 2805, 2
White, R. L., & Long, K. S. 1991, ApJ, 373, 543
Yusef-Zadeh, F., & Mehringer, D. M. 1995, ApJ, 452, L37
Yusef-Zadeh, F., Melia, F., & Wardle, M. 2000, Science, 287, 85
Yusef-Zadeh, F., & Morris, M. 1987, ApJ, 320, 545
Yusef-Zadeh, F., Roberts, D. A., Goss, W. M., Frail, D. A., & Green, A. J. 1996, ApJ, 466, L25
———. 1999, ApJ, 512, 230
Yusef-Zadeh, F., Uchida, K. I., & Roberts, D. 1995, Science, 270, 1801